THE NOISE OF AIRCRAFT

by

H. S. Ribner

General Lecture
Fourth Congress of the International Council
of Aeronautical Sciences

Paris, France
August 24 - 28, 1964

AUGUST, 1964

UTIAS REVIEW NO. 24
AFOSR 64-1310

ACKNOWLEDGEMENT

The assistance of J. Atvars, B.M. Nayar, L.K.O. Schubert, and T.O. Siddon in collecting and reviewing material for this paper is much appreciated. Support was provided under Air Force Office of Scientific Research Grant AFOSR 223-64. Unpublished experimental work by Atvars, Schubert and D. Strong (briefly mentioned) was supported also under grants of the National Aeronautics and Space Administration and the National Research Council of Canada.

ABSTRACT

Our understanding of the noise from jets, compressors, boundary layers, and sonic booms is still developing. In this lecture current concepts are presented, drawn in part from recent theoretical and experimental research. Where possible simple physical models of the major features of the noise and vibration phenomena are given. The noise from combustion and from propellers and rotors, being better known, is dealt with more briefly. Some mention is made of acoustical fatigue.

TABLE OF CONTENTS

NOTATION

1. INTRODUCTION (and throughout)

db	decibels: measure of sound pressure level $[20 \log_{10} (p_{rms}/p_{ref})$; $p_{ref} = 0.0002$ microbar$]$

2. COMBUSTION NOISE

c_o	ambient sound speed
P	acoustic power
V	volume flow
ρ_o	ambient density

4. COMPRESSOR NOISE

b	number of blades
c	sound speed
k	arbitrary integer
n	harmonic number
s	blade spacing
T	period
τ	time delay (s/U)
U	rotor speed
U_s	trace speed of rotor interaction mode
V_r	resultant flow speed at stator blade
v_n	wake velocity defect in nth harmonic

5. JET NOISE

C	convection factor (Eqn. (10))
c_o	ambient sound speed
D	nozzle diameter

f	frequency
L	effective scale of sound-generating eddies of dominant frequency f
M_c	eddy convection speed/ambient sound speed
P	acoustic power
$\overline{u^2}$	mean square turbulent velocity in element dV
U	local time-average flow speed
U_j	nozzle flow speed
V	effective volume of turbulent region
y	axial distance from nozzle
α	constant ∽ (eddy lifetime)$^{-1}$
θ	angle between sound ray and jet axis
$\bar{\rho}$	local time average density in jet
ρ_j	jet density at nozzle
ρ_0	ambient density outside jet

6. SONIC BOOM

a	local sound speed
$F(x)$	Whitham function (Eq. (14))
$h(x)$	height of centroid of S(x) above axis
$L(x)$	integrated lift from nose to x
M	flight Mach number (V/a)
M_c	climb Mach number (V_c/a)
Δp	overpressure in bow wave
p_a	ambient pressure at airplane
p_g	ambient pressure at observer position (normally the ground)

q	dynamic pressure ($\frac{1}{2} \rho V^2$)
r	perpendicular distance from flight path to observer
$S(x)$	local cross-section area at x
$s(x)$	area cut by Mach plane (Fig. 17)
V	flight speed (normally level flight)
V_c	climb or descent speed
x	distance from nose of airplane measured parallel to flight velocity
x_1	running value of x in integral
x_o	value of upper limit to maximize integral (Eqn. (13))
β	$\sqrt{M^2-1}$
γ	angle of climb; also ratio of specific heats (taken as 1.4)
θ	angle of line $\underline{r}$ with downward vertical
μ	Mach angle ($\sin^{-1}(1/M)$)
ρ_o	ambient density

7. BOUNDARY LAYER NOISE

c	a velocity characteristic of plate material (Eqn. (29))
c_o	ambient sound speed
f	frequency
h	panel thickness
I	sound power radiated per unit surface area
k	wave number = $2\pi \div$ wave length ($k = \sqrt{k_1^2 + k_2^2}$)
$\underline{k}$	wave number vector ($\underline{k} = (k_1, k_2)$)
p	pressure disturbance (relative to ambient)
$\overline{p^2}(f)$	pressure spectral density (in terms of frequency)

$\overline{p^2}(\underline{k}, f)$	pressure spectral density (wave number and frequency)
$\overline{pp'}(x, x', \tau)$	correlation of pressure at two points with time delay
T	eddy lifetime (autocorrelation down to e^{-1} in time T)
x, x'	points along panel centerline
$\overline{y^2}(f)$	spectral density of panel flexural displacement(frequency)
$\overline{y^2}(\underline{k}, f)$	spectral density of panel flexural displacement (wave number and frequency)
$\overline{yy'}(x, x', \tau)$	correlation of panel flexural displacement at two points with time delay
U	flow speed just outside boundary layer, or on centerline of 'equivalent' duct; in eqn. (22), jet centerline mean velocity at impingement point
U_c	mean convection speed of boundary layer wall pressure fluctuations
u	rms turbulent velocity; also (Secs. 7.5 - 7.7) phase velocity of pressure wave in direction $\underline{k}$
v	velocity of free flexural waves on panel
Γ	transfer function (admittance) (eqs. (24) or (26)).
η	panel damping coefficient (fraction of critical damping)
ρ	local density (mean)
ρ_0	ambient density
ρ_{SL}	sea level density
τ	time delay
τ_w	wall shear stress
φ	angle of pressure wave normal with respect to flow direction

1. INTRODUCTION

The noise of an aircraft arises almost entirely from the airflow about the vehicle and its parts. Hence the name aerodynamic noise has come into widespread usage. Lighthill has recently summarized a major part of the underlying theory [1, 2] with great clarity in his Bakerian Lecture [3]. There the fundamental aerodynamic mechanisms provided the unifying theme. Here, as indicated by the title, our objective is different and the unifying framework is the aircraft itself. We use the term aircraft in its broadest sense to include even spacecraft in their air-traversing phases. Thus the scope encompasses some phenomena - e.g. separated flow - of special importance for launch vehicles. Moreover, skin vibration is discussed at length because of its relevance to both noise and structural fatigue.

It will be convenient to start with a tabular breakdown of the major sources of aircraft noise:

EXCITERS

COMBUSTION PHENOMENA
PROPELLERS, ROTORS, FANS
JET FLOW
SONIC BOOM
BOUNDARY LAYER FLOW (FIG. 1)
- Attached Boundary Layer
- Separated Flow
- Oscillating Shocks

TRANSDUCER

SKIN VIBRATION (excited by the others, especially jet and boundary layer flow)

The "exciters" for the most part generate sound directly. Moreover, the unsteady pressure field near the exciters - the acoustic near field or 'pseudosound' [4] - can promote strong vibration in the aircraft skin. The vibrating skin in turn acts as a sounding board "transducer" to radiate a secondary sound. Within the aircraft cabin the secondary sound predominates. When the excitation arises from close-mounted propellers or jets, separated flow, or oscillating shocks, the large vibration amplitude can lead to fatigue cracks and failure (cf. Table I [5 - 8]).

Many features of flow noise have been discussed in terms of simple sources, dipoles, and quadrupoles [3]. Physical models of these elementary sound sources are shown in Fig. 2 [9]. Typical are the pulsating sphere to represent the simple source, the fluctuating force for

the dipole, and the fluctuating force pair - arising from a stress - for the quadrupole. Cancellation effects in the dipole and quadrupole result in progressively decreasing efficiency at the lower frequencies. If one assumes a sphere deforming or moving as in the figure at a frequency having a wave length of twice the sphere's circumference, the relative efficiencies are, simple source: dipole: quadrupole = 1: 1/13: 1/1000 ([7] , p. 33-4). The disparity decreases with increasing frequency as the reaction to the motion or deformation becomes more and more localized; at very high frequencies the efficiencies are equal ([10] p. 325). Further references to these elementary sound sources will be made in later sections.

2. COMBUSTION NOISE

The explosive sounds of piston engines and pulse jets are the major combustion noises of aircraft. (Turbulent combustion and rough burning - which produce entropy fluctuations [11, 12] - may be mentioned, but ordinarily they are not significant contributors.)

For the piston engine the pulsating exhaust flow can be approximated as a simple source mechanism. If the volume flow is V(t), the effective source strength is $\rho_o \ddot{V}$ and the acoustic power output may be written [3]

$$P = \rho_o \ddot{V}^2 / 4\pi c_o \qquad (1)$$

This is an approximation only, being applicable for wave lengths large compared with the exhaust port circumference. For more accuracy a Fourier analysis of V(t) into a fundamental and harmonics may be made. Equation (1) will fail for the higher harmonics, and for these the sound power may be calculated in terms of the radiation behavior of the port opening of area A ([7] p 33 - 20, [10] p. 325). The lower harmonics described by (1) will be non-directional, but the higher harmonics will show enhanced emission in the flow direction [13] .

The pulse-jet noise emission can likewise be approximated by (1), with V referring to the exhaust pulsations [14] . However, the inlet pulsations behave like a second weaker source, and the phasing provides a small distortion from uniform directivity. Theoretically the pulsations in momentum flux [3] behave somewhat like a dipole in enhancing the downstream directivity.

Piston engine exhaust noise can be lowered considerably through the use of mufflers. Only the straight-through type is used, to minimize back pressure. Such a muffler is the acoustical analog of an electrical band attenuation filter, and may be of the series or parallel type ([7] p. 33-21 and Ch. 21). The theory is, however, oversimplified by neglect of through flow and shock waves and predicts far better attenuation than is obtained [15] . The theory is nevertheless a useful guide to muffler design.

3. PROPELLERS AND ROTORS

Propeller noise generally dominates over the combustion noise. The sound consists of discrete tones at the blade passage frequency and its harmonics, together with a broad band noise that predominates above 1000 cps ([7] p. 33-17). In the Gutin theory of the discrete tones [16-18] the rotating blade forces are Fourier analyzed over the propeller disc into rotating sinusoidal waves. Each rotating wave pattern, resolved into thrust and torque components, is harmonic in time at stationary points. Known formulas [19, 20] for the sound radiated by an oscillating force (dipole sound, Fig. 2) lead to an integral over the swept disc for the resultant sound field. In more recent developments [21-23] the forward speed and blade load distribution are allowed for.

The phasing around the propeller disc gives rise to a characteristic four-lobe directivity pattern. An example is shown in Fig. 3 ([7] p. 33-16). Here two very small lobes are directed forward at roughly 45^{o} to the axis and two large lobes lie at roughly 100^{o} to 135^{o}. The sound pressure field actually spins about the propeller axis as if rigidly attached to the propeller, and the lobes represent the rms effect in any plane through the axis.

The broad band noise - often called vortex noise - is related to the Aeolian tones emitted by a rod in a wind. The lift oscillates in sympathy with the shedding of a Karman vortex street, generating dipole noise of a characteristic frequency (see, e.g., [25]). The rotating propeller blade behaves similarly, but the radial increase in velocity from hub to tip causes the local shedding frequency to follow suit on the average, giving a continuous distribution of sound frequency, ([7] p. 33 - 17).

In principle helicopter rotors can be analysed on the same basis as propellers. However, the discrete frequencies are weak and in hovering are masked by strong engine and gearing noises persisting up to the order of 1200 cps. Above this frequency the broad band noise predominates [26] . This probably consists only in part of vortex-shedding noise: the remainder is presumably caused by fluctuations of blade lift associated with the passage through the turbulent wakes of upstream blades (see Section 4. "Compressor Noise").

4. COMPRESSOR NOISE

4.1 General Remarks. - The noise from the compressor or fan in a turbojet can compete with the jet noise. When an aircraft comes in for a landing an observer below the flight path hears two maxima - one slightly before the aircraft is overhead and one after it has passed [27] . The first peak is due to fan noise radiated from the engine intakes. This high pitched compressor whine can be more irritating than the relatively low pitched rumble of a jet at take-off. Moreover, with the present trend

toward fan-jets (bypass jets) there is a trade-off between reduced jet noise and increased fan or compressor noise.

The axial-flow fan used as an aircraft compressor bears a family resemblance to a propeller; however, it resembles a cascade of airfoils even more. Like a propeller it generates discrete tones and broad-band noise, the basic mechanisms being in part the same. In both cases the discrete tones are associated with the pressure fields that spin about the axis of rotation.

Propeller noise theory is inapplicable to fans - it can greatly underestimate the noise - because, unlike the propeller, the fan is housed in a duct. For the discrete tones we must consider a two part process: propagation of the spinning modes along the duct, and radiation from the end of the duct - in practice the inlet.

4.2 Duct Cut-off Effect - These features have been treated theoretically and experimentally in a classical paper by Tyler and Sofrin [28] . A major finding is that the more slowly spinning pressure modes can decay exponentially in their passage through the duct. This is the cut-off effect. The criterion for cutoff may be stated as follows: a spinning pressure-field mode will decay if the linear speed at a certain reference radius is subsonic (Fig. 4). The reference radius depends on the mode shape and in a calculated instance it agrees with the center of gravity of the radial pressure plot. Note the analogy with aerodynamic flow over a wavy wall: for subsonic flow the pressure field decays exponentially with distance from the wall; for supersonic flow the pressure field propagates in the form of Mach waves without decay (in the approximation of linear theory).

4.3 Radiation from Duct. - The supersonically spinning modes propagate without change of amplitude or wave shape to the end of the duct. There the particle velocities in the pressure wave may be simulated by an assemblage of elemental pistons over the duct face. The pattern rotation gives a sinusoidal oscillation to each of the pistons, and they radiate sound like simple oscillatory sources [10] . The joint radiation from the assemblage requires an integration, with due regard for phase, over the duct face. The mathematical formalism due to Tyler and Sofrin [28] closely resembles Gutin's treatment [16] for propellers, but with simple sources replacing dipoles. The resultant pressure field is again a spinning pattern as for a propeller. The theory shows satisfactory agreement with experiment.

The cited analysis for a round or annular duct neglects the effect of axial flow through the duct on the attenuation and propagation. A two-dimensional cascade analysis of Bragg and Bridge [29] (see later), although oversimplified as compared with a duct, does allow an estimation of the effect of through flow. In this model the analog of a supersonically spinning mode radiates less effectively upstream as the through flow is

increased "which blows the sound back again". At choking the radiation is zero. Thus as rotor rpm is increased the radiation is predicted to increase from zero at duct cutoff quickly to a maximum followed by a slow decay to zero again at high rotor speed (choking) (Fig. 5) [29].

4.4 Rotor-Stator Interaction. - An isolated fan rotor will generate modes spinning solely at the rotation frequency. The rotor wakes impinging on a stator will generate a large number of interaction modes from fluctuating lift on the stator blades. These modes will spin at different rates, some forward and some backward, according to certain phasing effects. Submultiples as well as multiples of the rotor rotation frequency occur [28 - 30]. Those of the submultiple-speed modes moving subsonically (at the reference radius for the mode) will decay exponentially as they pass through the duct due to the cutoff effect.

This behavior may be demonstrated on a two-dimensional model (Fig. 6). The following treatment is slightly modified from that of [29]. The rotor wakes impinge on a given stator blade at the blade-passage frequency U/b, generating fluctuating lift and sound at this frequency and its harmonics. The stator blades constitute an array of oscillating dipoles with successive phase shifts arising from the spacing s between blades, giving a time delay s/U. As the sound waves radiate out from each dipole they will tend to form fronts where the joint effects are in phase. For two adjacent dipoles this condition is illustrated by the geometry of the figure. This gives (with k an arbitrary integer)

$$s \cos \alpha = ckT - c\tau$$

where τ is the time delay s/U, and kT corresponds to k periods; kT = kb/nU for the nth harmonic of the rotor wake pattern. It follows that

$$\cos \alpha = \frac{c}{U}\left(\frac{kb}{ns} - 1\right) \qquad (2)$$

describes the inclination of wave normals. The wave pattern moves with a speed $U_s = c/\cos \alpha$ along the blade row,

$$\frac{U_s}{c} = \frac{U}{c}\left(\frac{kb}{ns} - 1\right) \qquad (3)$$

This demonstrates the multiplicity of speeds U_s of the interaction modes as compared with the single speed U for the rotor modes.

When U_s is less than the speed of sound, c, α is imaginary and the postulated wave pattern does not exist. A proper pattern would then show the exponential decay predicted for the duct cutoff effect. Equation (3) shows how the interaction modes may include slow-moving members ($|U_s| < U$) that will cutoff before the rotor modes.

4.5 Magnitude of Interaction Tones [29] . - Estimates show that blade incidence changes associated with wake-cutting dominate the production of rotor-stator interaction tones. Potential flow interactions are much weaker except at small separations. For a given compressor the estimate gives

$$\frac{\text{acoustic power}}{\text{mass flux}} \sim Bn^2 \left(\frac{v_n}{V_r}\right)^2 \frac{U^5}{c^3} \qquad (4)$$

for the nth harmonic of the wake pattern and B blades. Here v_n/V_r is the angle of attack fluctuation when the wake velocity defect is v_n in the nth harmonic, and U is the blade rotation velocity. For a typical design the proportionality constant in (4) is 0.03. On inserting estimated values for the fundamental tone n = 1, $v_n/V_r = 0.2/\sqrt{3}$, U = 550 ft/sec., c = 1100 ft/sec., the equation gives

0.13 watt per lb/sec flow

as the specific acoustic power output for a typical compressor. According to (4), this acoustic output will increase as the fith power of blade speed and second power of the wake velocity defect for fixed compressor mass flow.

Experimentally it is found that the energy radiated upstream in the discrete tones from successive stages of a compressor decreases by about a factor of two per stage. This is presumably accounted for by reflection processes, etc., whereby a stage attenuates the sound passing through. Thus the first two stages account for three-fourths the total sound power, and the remaining stages may therefore be neglected in practical computations of inlet noise.

4.6 Broad Band Noise. - The broad band noise depends on random processes. One source is turbulence in the approach stream which yields fluctuating angles of attack and hence fluctuating lift [31 - 33] . A second source is the unsteady lift associated with vortex shedding (Aeolian tones are generated when the shedding is periodic) (e.g. [25]). Still a third is the noise radiated by the turbulent boundary layer on the blades, with or without blade vibration (see Section 7, Boundary Layer Noise.) Their relative effectiveness is estimated in [33] . Although the second of these dominates in the broad band noise of helicopter rotors, the first is considered to dominate in compressor noise. Here the chief sources of stream turbulence are probably the turbulent blade wakes and wall boundary layers. Roughly speaking the broad band noise in a one third octave band is estimated as having about one half the energy of a discrete tone centered in the band [29] .

4.7 Control of Compressor Noise (cf [29]). The ability of the duct to cut off radiation from subsonically spinning discrete tone modes might be exploited in the design stage. The parameters are the respective numbers of rotor and stator blades, duct length, etc. However, the inevitable presence of many supersonically spinning interaction modes must be taken into account. The use of acoustically absorptive filters in the inlet is not a promising method of control, it is argued, because of dimensional and other practical considerations. On the other hand, choking the inlet will indeed block passage of the compressor sound: this is well known. However, the choking control mechanism - e.g., an axially movable centerbody - gives rise to some complexity. Careful attention in design to the wake impingement process and other sources of turbulence may reduce the discrete tones and broad band noise. However, more needs to be known of the flow details, and also of the acoustic interference between blade rows.

5. JET NOISE [9]

5.1 Mechanisms. - The fluctuations in momentum flux in a turbulent jet flow give rise to inertial forces. These unsteady forces may be thought of as occurring in opposed pairs since the resultant force field must be zero. A fluid element subject to such a force pair or stress suffers a fluctuating quadrupole deformation (Fig. 2(c)): this Lighthill's well known mechanism of aerodynamic sound generation [1-3, 34] .

Associated with the inertial forces will be pressure gradients in the flow. A region of high pressure will be slightly compressed and conversely (Fig. 7). The transient local compressions and expansions (dilatations) throughout the jet behave like tiny pulsating balloons and constitute an alternative source-like mechanism of sound generation (Fig. 2(a)). Mathematically, the dilatation and quadrupole mechanisms are equivalent in the sound they produce when summed over the region disturbed by the flow [12, 34] .

The fluctuating local pressure (or alternatively the quadrupole strength) is of order $1/2\ \rho u^2$, the stagnation pressure of a turbulent eddy. The sound generation process involves a further operation $\partial^2/\partial t^2$ because fluid acceleration is involved. Each operation $\partial/\partial t$ is equivalent to multiplication by the dominant frequency f, giving the acoustic source strength as $\sim \rho \overline{u^2} f^2$ effectively. The acoustic power emission depends on the square of this source strength: more specifically, the sound power radiated from a volume element dV of turbulence of effective scale L and mean square velocity u^2 is

$$dP \sim dV\ \rho_o (\overline{u^2})^2 f^4 L^3 / c_o^5 \qquad (5)$$

approximately, where ρ_o is the density and c_o is the speed of sound, assumed spatially uniform. Here L^3 represents the volume of a coherently radiating 'eddy' of turbulence. The equation implies that each eddy radiates independently: the radiation from each is statistically independent.

5.2 U_j^8 and Other Similarity Laws. - In an idealized jet flow we assume that the turbulent velocity scales with the local mean velocity, $u^2 \backsim U^2$, and frequency $f \backsim U/L$, with the result

$$dP \backsim dV\ \rho_o U^8/L\ c_o^5 \tag{6}$$

For the jet as a whole we may take $dV \backsim D^3$, $L \backsim D$, $U \backsim U_j$ to obtain the total power as

$$P \backsim \rho_o U_j^8\ D^2/c_o^5 \tag{7}$$

where U_j is the nozzle velocity, D the diameter. This is Lighthill's famous U^8 law which agrees with experiment over a noise power range of a million to one.

Consider the sound power emission from successive slices dy (Fig. 8) of the jet taken normal to the axis; in this case U and L are taken as typical for the slice. The effective region of the slice occupied by the turbulence is dV. For the mixing region (to the end of the potential cone) we assume $dV \backsim y\,D\,dy$ (annulus), $L \backsim y$, $U \backsim U_j/2$ = constant. For the fully developed jet we assume $dV \backsim y^2\,dy$ (disc), $L \backsim y$, $U \backsim U_j D/y$. Insertion into (6) gives [36, 37]

$$\frac{dP}{dy} \backsim \frac{\rho_o U_j^8 D}{c_o^5} \begin{cases} (y/D)^0 & \text{mixing region} \\ (y/D)^{-7} & \text{developed jet} \end{cases} \tag{8}$$

for the distribution of sound power emission with distance y measured along the jet axis (Fig. 8). The very fast decay (like y^{-7}) in the developed jet implies that the first eight diameters or so of the jet radiate the bulk of the noise.

For simplicity we may imagine that a given slice dy of the jet emits just a single characteristic frequency that is lower the farther the slice is from the nozzle: the actual rather peaked spectrum of the slice is thus considered squeezed into a single line. Then the spectrum emitted by the jet as a whole can be approximated by the construction of Fig. 8, wherein we assume $f \backsim U_j/y$ in the mixing region and $f \backsim U_j D/y^2$ in the developed jet for reasons of dynamical similarity. The results are [38]

$$\frac{dP}{df} \backsim \begin{cases} \dfrac{\rho_o\ U_j^9\ D}{c_o^5}\ f^{-2} & \text{mixing region (high end of spectrum)} \\ \dfrac{\rho_o\ U_j^5\ D^5}{c_o^5}\ f^2 & \text{developed jet (low end of spectrum)} \end{cases} \tag{9}$$

for the slope of the frequency spectrum on either side of the peak.

5.3 Self-Noise and Shear Noise. - A more detailed analysis indicates that the 'self-noise' due to the turbulence is accompanied by 'shear-noise' due to cross-coupling with the mean flow [1-3, 34, 37] . This can be seen [39] on writing the flow velocity in direction x as $u_x + U_x$, the sum of a turbulence component and a mean value. Then, on squaring to obtain momentum flux as used in one form of the quadrupole theory [40] , one obtains u_x^2 and $2u_x U_x$ as effective noise generators. The first term yields the self-noise and the second term - whose integral vanishes if there is no shear - yields the shear noise.

In the theory of [39] the 'shear noise' spectrum is peaked an octave below the 'self-noise' spectrum and has a relative strength $\backsim \cos^4\theta$, where θ is the angle of emission relative to the flow direction (y-axis). The low frequency 'shear-noise' spectrum dominates at small values of θ (e.g. 30°) and the high frequency 'self-noise' spectrum dominates near 90° where $\cos^4\theta \to 0$ (Fig. 9; other features of the figure are explained below.)

5.4 Convection, Refraction, Density and Temperature. - Convection of the eddies by the mean flow (when subsonic) crowds the sound waves in the downstream direction. This causes an effective Doppler shift of frequency in the ratio C^{-1} and an associated amplification C^{-4} where [12, 41]

$$C = \left[(1 - M_c \cos\theta)^2 + \alpha^2 M_c^2\right]^{\frac{1}{2}}, \qquad (10)$$

M_c is the convection speed/c_o and α is inversely proportional to the lifetime of an eddy. Thus, as shown in Fig. 9, convection shifts points of the spectrum upward and toward the right. A progressive leftward increase in the vertical shift C^{-4} is hypothesized, arising from a variation of M_c along the jet. This would distort the 30° spectrum (top curve) so that the peak lies further toward the left, despite the Doppler shift C^{-1} of the individual spectrum points toward the right [39] . An "anomalous" leftward shift of this kind is observed experimentally as well as the difference shown between spectrum at 30° and 90°. In all this the abscissa scale is $\backsim f/U_j$ to allow for the increase of frequencies in the turbulence with velocity. Thus the leftward shift of the peak implies the peak frequency increases more slowly than U_j. Empirically f_{peak} varies about like $U_j^{1/2}$.

The overall effect of convection, obtained e.g. by integration of the spectrum, is given by the directional amplification C^{-5}. This modifies the basic $1 + \cos^4\theta$ directivity to beam the sound into a broad fan pointing downstream. Opposing this, the mean jet flow refracts the rays outward to give a pronounced valley of low intensity at the heart of the fan. The resultant directional pattern peaks strongly at an oblique angle (e.g., 40° for turbojets, 20° for cold air jets) to the flow direction (Fig. 10). The

figure shows also refraction measurements made recently in our laboratory with a harmonic "point" source of sound placed in a jet [42] *. The next figure (Fig. 11) shows how well the factor $(1 + \cos^4\theta)\, C^{-5}$ - which is dominated by the convection effect - agrees with experiments on turbojet directivity outside the refraction valley.

The larger the extent of the jet (region of sensible velocity) compared with a wave length of sound the more refractive effect it should have; the cited experiments confirm this. The effect on the jet noise appears as an increase in the refraction valley - an outward rotation of the peak intensity - with increasing frequency.

An outward refraction of the sound rays is also to be expected when the speed of sound in the jet is above ambient; this has likewise been measured with a "point" source [42] . Correspondingly a large outward rotation of the peak intensity of jet noise is found for a three-fold increase in the speed of sound [45] .

If the local jet density $\bar{\rho}$ differs from ambient there should be a multiplicative factor $\bar{\rho}^2/\rho_0^2$ for the noise emission (5) from unit volume. Experimentally, the emission is closely proportional to ρ_j^2/ρ_0^2 where ρ_j is the density at the nozzle; this ratio differs more from unity than $\bar{\rho}^2/\rho_0^2$ because ρ_j is not diluted by mixing. We refer here to a jet of one gas issuing into another more or less isothermally.

When the jet consists of heated air issuing into air the change in jet density or temperature appears to have no measurable effect on total noise power. The writer suggests that turbulent heat transport generates additional sound from entropy fluctuation, offsetting the reduction associated with reduced density [9] .

5.5 Reexamination, and Extension to Supersonic Jets. - The low-speed derivation of a U_j^8 noise power law was based on an inaccurate model of jet flow. A reevaluation should employ rms turbulent velocity $\sim U_j^{3/4}$ approximately (from subsonic experiments) to yield close to U_j^7. This must be multiplied by the convection factor C^{-5}, averaged over direction. This average (Fig. 12) exhibits a slow rise to a moderate peak for convection speed $U_j/2$ near sonic. For $\alpha \simeq 0.55$ the product with U_j^7 is not far from U_j^8 over most of the subsonic range. On proceeding to supersonic convection speed the mean convection factor decays like U_j^{-5}. (This reflects a change in the generation process wherein eddy Mach waves are dominant [41, 46]). If the U_j^{-5} is multiplied by a hypothetical U_j^8 basic emission the result is a U_j^3 law. Experimentally, the data for subsonic convection speeds (model jets, turbojets) very accurately follow a U_j^8 law, and there

* Eldred et al. [43] have had some success in estimating the refraction valley by means of a ray tracing technique. Their results are more realistic than those from analytic procedures based on infinite nonspreading "jets" (e.g. [44]).

is a transition at supersonic speeds (afterburning jets, rockets) to something approximating a U_j^3 law for the limited region of the data (Fig. 13).

Division of the two-slope sound power law $U_j^8 - U_j^3$ by the kinetic power of the jet $\backsim U_j^3$ gives a two-slope efficiency $\backsim U_j^5$, and constant. Thus the steep rise for subsonic jets levels off to a constant limiting efficiency (of 0.3 to 0.8%) for rockets.

The experimental rocket data do not extend beyond $U_j \simeq 8\, c_o$ (the effective eddy speeds are much less) and the use of the convected quadrupole (or dilatation) deductions for higher speeds is purely speculative, as has been indicated. The approach of O. M. Phillips [46] - an asymptotic theory for high values of U_j/c_o - predicts that the efficiency must ultimately diminish like $U_j^{-3/2}$.

5.6 Control of Jet Noise. - Substantial reduction in jet noise can be accomplished, for a given thrust, by the reduction in velocity associated with a larger jet diameter according to the U_j^8 law. This is exploited in the increasingly popular bypass or turbofan engines. In the bypass engines now entering service noise reductions of about 10 to 12 decibels are achieved for the same power. The penalty is emergence of compressor whine as a nuisance in the landing approach.

Corrugated and multi-tube nozzles are the most widely used means for quieting existing turbojets. Their development has been motivated by conflicting interpretations of the theory, and the explanation of their behavior remains a matter of controversy and speculation. It is generally agreed that reduction in shear plays an important role, presumably reducing overall turbulence levels: these nozzles entrain external air into a restricted region between the corrugations or sub-jets, giving it some forward velocity. Another notion is that the sound from one small jet (or corrugation) is reflected and refracted ('shielded') by the temperature and velocity field of nearby jets so that the aggregate sound has a less peaky directional distribution [47] .

A group headed by R. Lee of General Electric has had some success with a semi-empirical computerized method for predicting muffler behavior (and flow development of interfering jets) in some detail [48] . Eldred et al. [43] have recently gone further in this direction with somewhat different methods, and they show rather impressive agreement with experiment for muffler behavior.

6. SONIC BOOM

6.1 Boom Mechanism, Refraction, and Focusing. - An airplane in supersonic flight carries along a bow shock and tail shock that "slide(s) over the eardrums of the residents on airways" [49] (Fig. 14). At the ground these two shocks have normally evolved into the classical N-wave asymptotic shock pattern (Fig. 15). This 'pressure signature'

sweeping over the observer is similar to that from an explosion and produces a similar 'boom' in the ear. If the separation between the bow and tail shocks is relatively large - as for a large airplane (bomber) - two booms are heard. For a small separation - as for a fighter airplane - only a single boom is heard, as the ear cannot resolve impulses that are too closely spaced in time.

There exists a 'cutoff Mach number' for the flight speed, below which the shock pattern will not reach the ground. This boom-free condition results from atmospheric refraction due to the temperature gradient, and (slightly) the wind. The cutoff occurs when the ground speed of the shock pattern, corrected for wind gradient, just matches the speed of sound at the ground [50] . It is clear (Fig. 16) that the speed V_c in a climb is greater than the level-flight speed V, for cutoff. Moreover, at altitude the sonic speed a is lower than the sonic speed a_g at ground level. Thus by geometry the cutoff Mach number for level flight, V/a, exceeds unity. More specifically (e.g. [51]),

level cutoff: $$M = V/a = a_g/a \qquad (11)$$

climb cutoff: $$M_c = \frac{V_c}{a} = \frac{M}{\cos\gamma - \sin\gamma\sqrt{M^2 - 1}} \qquad (12)$$

Examples for flight just above the tropopause (about 36,000 ft.) give the respective cutoff values,

$M = 1.15$ for level flight
$M_c = 1.57$ for climb at $\gamma = 21^o$
$M_c = 1.01$ for descent at $\gamma = -21^o$

The favorable effect of climb is evident.

The remarks so far have referred to flight at constant speed. Curved flight paths and linear acceleration provide possibilities for focusing or defocusing the shocks. The implications for modifying boom intensity in this way have been studied by a number of authors [52 - 58] . It appears that the problem will be discussed in some detail elsewhere at this Congress, so it will be passed over here.

6.2 N-Wave Development: Volume Effects. - The prediction of the intensity and geometry of the far-field N-wave is traceable to a classic paper by Whitham [59] . It was already known from shadowgraphs of bullets, (e.g. [60]) that $r^{-1/2}$ law of decay with distance (r) calculated from linearized theory was incorrect. Moreover, instead of being straight and parallel as in the linearized theory, the bow and tail waves are shocks that diverge with distance (Figs. 14, 15). Whitham showed how the essential nonlinearity of the process can be allowed for by a modification of linear theory: this led to the more rapid $r^{-3/4}$ law of decay of intensity with dis-

tance and an $r^{1/4}$ law for the divergence of the front and rear shocks. Both laws have been well verified by experiment (e.g. [61]).

It follows that the area under the positive pressure pulse of the N-wave is proportional to $r^{-3/4}$ (for height, Δp) times $r^{1/4}$ (for length). This gives an impulse strength $\backsim r^{-1/2}$ just as in the linear theory [49] . The $r^{1/4}$ stretching of the N-wave has been offset by an $r^{-1/4}$ reduction in overpressure Δp.

Whitham's result for the overpressure in the bow shock of a non-lifting slender axisymmetric body may be written (slightly generalized) as (e.g. 51)

$$\frac{\Delta p}{\sqrt{p_a p_g}} = \frac{2^{1/4}\gamma (M^2-1)^{1/8}}{(\gamma+1)^{1/2} r^{3/4}} \sqrt{\int_0^{x_0} F(x)dx} \qquad (13)$$

where $$F(x) = \int_0^x \frac{S''(x_1)}{\sqrt{x-x_1}} dx_1 \quad \text{(volume only)} \qquad (14)$$

with x_0 chosen to maximize the integral. Here S is the local cross-sectional area at x_1 and primes denote differentiation; moreover [57] $\sqrt{p_a p_g}$ replaces p to allow for the atmospheric pressure gradient. To be more exact in the application to aircraft a form of the supersonic area rule [62] should be used [63, 64] : $S''(x_1)$ is determined from

$$S(x_1) = s(x_1) \sin\mu \qquad (15)$$

where $s(x_1)$is the area cut by a Mach plane as in Fig. 17. This applies when the observer is directly below the flight path, assumed horizontal. When the observer is in a plane through the flight path making an angle θ with the vertical (polar coordinates are r, θ) the Mach plane must be rotated about the x_1 axis through the angle θ: this generalizes s and S to $s(x_1, \theta)$, $S(x_1, \theta)$, respectively. Thus the far-field shock due to the volume displaced by the airplane is locally the same as that of a certain equivalent body of revolution. This equivalent body defined by $S(x_1, \theta)$ varies, however, with the inclination θ of the flight path-to-observer plane.

6.3 N-Wave: Lift Effects. - Extension to the case of a lifting wing-body configuration is generally credited to Walkden in a very comprehensive paper [63] , although alternative treatments by Busemann (an approximation) [49] , Warren and Randall [59] , and Morris [64] should be mentioned. We cite the most recent form due to Randall [65] . He represents a "smooth slender" aircraft in terms of a line distribution of sources and multipoles along the axis. In the far field the sources dominate the effect of volume and the dipoles dominate the effects of lift and volume displacement. The result is a generalization of (14) to the form

$$F(x) = \frac{1}{2\pi}\int_0^x \frac{S''(x_1) + \beta\left\{\frac{L''(x_1)}{2q} - [S(x_1)h(x_1)]'''\right\}\cos\theta}{\sqrt{x - x_1}}\,dx_1 \qquad (16)$$

Here $\beta = \sqrt{M^2 - 1}$, $q = \frac{1}{2}\rho U^2$, $L(x_1)$ is the integrated lift from the nose to x_1 and $h(x_1)$ is the height of the centroid of $S(x_1)$ above the axis. Thus lift is accounted for by the L'' term and volume displacement (due to incidence or camber) by the S h term. Cos θ varies from +1 directly below the airplane to -1 directly above (the sign convention here is opposite to that of [65]) exhibiting the antisymmetry of the lift effect.

The earlier papers do not include the displacement term, although Walkden [63] does augment the lift term by a wing-fuselage interference term. The form (16) incorporated into (13) without the displacement term, and with $\theta = \pm 1$, has shown reasonably good agreement with both wind-tunnel and flight tests [61] . The validity of the displacment term remains to be tested.

The equations show - because of the square root and the dependence of the limit x_o on both - that the volume and lift affects do not combine linearly. However, the respective Mach number dependences are of interest (Fig. 18). (For this purpose note that $\beta/2q = \sqrt{M^2-1}/\gamma M^2 p_a$). Similarly the respective altitude dependences may be exhibited (Fig. 19). The extra factor $p_a^{-\frac{1}{2}}$ in $\beta/2q$ accounts for the slower decay of lift effects with altitude. This figure shows that as aircraft grow bigger and are thus forced to higher altitude to minimize the boom, lift becomes relatively more important.

7. BOUNDARY LAYER NOISE

7.1 Generation Process: Rigid vs. Flexible Walls. - There are two mechanisms by which a turbulent boundary layer can create noise as it passes over a solid surface. If the surface is rigid the turbulent pressure fluctuations in the flow radiate sound directly into the adjacent air. If the surface is flexible, the fluctuating pressure field of the boundary layer can excite flexural vibration in the surface. The vibrating surface then acts as a radiator of sound similar to the diaphragm of a loudspeaker. Both mechanisms are present for a flexible wall.

The flexure mechanism will ordinarly dominate in aircraft cabin noise at subsonic speeds [66] ; therefore we shall comment only a little on the rigid wall mechanism. Curle [20] has extended Lighthill's theory of the generation of aerodynamic noise [1, 2] to allow for the presence of a wall. The formulation allows the radiation to be expressed in terms of a distribution of quadrupoles (like those of jet noise) throughout the boundary layer and a surface distribution of dipoles of strength proportional to the fluctuating pressure (e.g., [3]). It is now agreed after much dis-

cussion (e.g. [67 - 72]) that the integrated dipole strength must vanish for a large surface, which implies a sort of pairing of opposed dipoles to behave like quadrupoles. The radiated sound power per unit area of surface has been recently evaluated in [72] as

$$I = 5 \times 10^{-4} \ \rho_o U^8 / c_o^5 \qquad (17)$$

approximately for low speeds, exhibiting a U^8 law characteristic of quadrupole aerodynamic noise. The effects of convection of the wall pressure field [3] and the additional radiation from the volume distribution of quadrupoles within the boundary layer are not taken into account; the latter is discussed in e.g. [73] .

7.2 Pressure Field Under the Boundary Layer (Pseudosound).- The unsteady boundary layer pressure field serves to drive the vibrations of a flexible wall or panel. Empirically [74 - 76] this pressure field has the character of a convected spatial pattern with relatively slow fluctuation as viewed by an observer moving with the pattern. A stationary observer will record a relatively fast fluctuation, due primarily to the motion of the pattern past him.

Theoretical evaluation of this pressure field (in statistical form) in terms of the boundary layer turbulence was initiated by Kraichnan [77] . More recent developments are summarized in [72] .

The pressure field in the low speed boundary layer has been called pseudosound [4]: the field is largely localized and arises from inertial effects with negligible influence of compressibility. The rms pressure amplitude at the wall is of the order of the stagnation pressure of an eddy. A typical pressure-producing eddy has about $7\frac{1}{2}\%$ of the stream velocity, whence the rms pressure is

$$p_{rms} \simeq (.075)^2 \ q \simeq 0.006 \ q \qquad (18)$$

where q is the stream dynamic pressure $\frac{1}{2} \rho_o U^2$. (This is a useful approximation [78] ; a more accurate expression relates the pressure to the wall shear stress τ_w as

$$p_{rms} \simeq 2.3 \ \tau_w \qquad (19)$$

at low speeds with an increase in the constant with Mach number to an apparent limiting value of about 5.5 or 6.0 [79] .)

On an acoustic decibel scale the pseudosound pressure level (18) (re. 0002 microbar) is

$$db = 104.5 + 40 \log_{10} (U/100) \text{ ft/sec} + 20 \log_{10} (\rho / \rho_{SL}) \qquad (20)$$

where ρ_{SL} refers to sea level air density. At 30,000 feet and 800 ft/sec, this comes to 132 decibels. This rather high intensity would be recorded

by a microphone flush mounted in the wall under the boundary layer. The microphone cannot distinguish between true radiated sound and pseudosound.

7.3 Jet Impingement, Separated Flow, and Oscillating Shocks. - We have employed the rather crude model

$$p_{rms} \simeq \tfrac{1}{2} \rho u^2, \tag{21}$$

equating the rms fluctuating wall pressure to the stagnation pressure of an effective average eddy characterized by rms velocity u. This gives the right order of magnitude for an attached boundary layer and tends to underestimate for a jet at grazing incidence.

When a jet impinges normally against a wall the fluctuating part of the peak wall pressure is expected to satisfy

$$p_{rms} \simeq \rho U u , \tag{22}$$

which is the difference between $\frac{1}{2} \rho (U + u)^2$ and $\frac{1}{2} \rho U^2 \equiv q$. As compared with (21) there is an apparent amplification 2U/u, twice the ratio of the stream velocity to the rms turbulence velocity. Experimentally* a maximum value of p_{rms} occurs when the plate is about 7 diameters from the nozzle. For this case low speed measurements give

$$p_{rms} \simeq 0.21\, q \tag{23}$$

in approximate agreement with the prediction of (22). Compared with a boundary layer flow with the same local q ($p_{rms} \simeq 0.006\, q$) a jet at normal impingement generates some 35 times the level of pseudosound.

The stream is largely stagnated in separated flow bubbles (Fig. 1) and (to a lesser extent) in blunt body wakes. Thus the rms fluctuating wall or base pressure may be expected to be intermediate between the predictions of (21) (smooth parallel flow) and (22) (impingement). Large pressure amplifications may be expected from this model and they are in fact observed [79]. The model is clearly an over-simplification, but it may be useful. It points up impingement and flow separation as probable strong exciters of vibration and noise, leading to serious danger of fatigue.

Comparative estimates of rms pressure for exciters of this same general nature (except the last) are listed in the following table (see also Table I at the end) [5]:

---

* Unpublished measurements by J. Atvars, L. K. O. Schubert (1963) and D. Strong (1964), Institute for Aerospace Studies, University of Toronto.

	p_{rms}/q
Base Pressure Fluctuations	0.015
Wakes From Protuberances	.015 - .07
Cavity Resonances	.03 - .06
Separated Turbulent Flows	.1
Oscillating Shock Waves	.3

The last phenomenon, oscillating shock waves, can arise at the ramp-like separation bubble in a supersonic boundary layer (Fig. 1), apparently from fluctuations of the separation point. The pressure jump through the shock as it oscillates produces large local rms pressure fluctuations, e.g., of the order of 0.3 q.

The oscillations of a plane shock about its mean position would give rise to an oscillatory line force of the same frequency and a line bending moment of double the frequency. Motivated by the possibility of structural fatigue, the flexural motion and stresses of finite and infinite panels excited in this way have been investigated [80, 81] . However, only the case of shock-free boundary layer excitation will be discussed in what follows.

7.4 Excitation of Panel Vibration. - The skin of an airplane is curved, continuous, and attached to ribs and stringers. So far this has not proved amenable to analysis for boundary layer excitation. Thus we idealize the skin as a succession of independent plane rectangular panels. Even this simplified problem is not yet fully solved [82 - 89] .

To start with, we refer to an even simpler problem, the excitation of panel vibration by a nearby jet; this is motivated by the structural fatigue aspect. The jet, if not too close, gives rise to a large scale fluctuating pressure field at the panel so that at any instant the pressure is reasonably uniform over the panel. Only the time history of this pressure is significant.

Figure 20 shows the pressure input to the panel as a random signal in time (cf. e.g. [90]). The vibration output shows a random amplitude but a definite periodicity: the panel is responding mainly at its fundamental resonant frequency. This is exhibited by the sharply peaked frequency spectrum. The pressure input, on the other hand, has a broad flat spectrum.

The output and input spectra are related by

$$\overline{y^2}(f) = \Gamma^2(f)\, \overline{p^2}(f) \qquad (24)$$

The 'transfer function' $\Gamma(f)$ measures the relative vibration amplitude when the pressure input is a single frequency f. $\Gamma(f)$ contains the resonant peakiness of the panel response. The mean square output and input are given by the areas under the spectral curves:

$$\overline{y^2} = \int_0^\infty \overline{y^2}(f)\, df; \quad \overline{p^2} = \int_0^\infty \overline{p^2}(f)\, df \tag{25}$$

When we go over from jet to boundary layer excitation the situation is much more complex (Fig. 21). The pressure field in the boundary layer can no longer be treated as spatially uniform. The scale of the pressure 'patchiness' corresponds to the dominant eddy size in the turbulence and is often small compared with the panel dimensions. The alternating up and down spatial distribution of force over the panel favors a corresponding type of deformation, that is, high order mode shapes. Thus a wide range of modes will be excited, not just the lowest one or two [82, 83] .

We can handle the spatial unevenness of the pressure field by going over to three-dimensional spectra. These are primarily applicable to infinitely large panels. We write the spectra in the form [82]

$$\begin{aligned} &\text{output,} && \overline{y^2}\,(\underline{k},\ f) \\ &\text{input,} && \overline{p^2}\,(\underline{k},\ f),\ k = 2\pi\ /\text{wave length} \\ & && \overline{y^2}\,(\underline{k},\ f) = \left|\Gamma(\underline{k},\ f)\right|^2\, \overline{p^2}\,(\underline{k},\ f) \end{aligned} \tag{26}$$

Here a new variable, the wave number $\underline{k}$, appears. The vector $\underline{k}$ arises in the decomposition of the random pressure field into spatial sinusoidal waves by Fourier analysis. Figure 22 shows an elementary pressure wave and exhibits the reciprocal relation between the wave number k and the wave length λ.

To obtain the ordinary one-dimensional frequency spectrum $\overline{y^2}(f)$ from (26) an integration from $-\infty$ to ∞ in k_1 and k_2 is required; a similar integration gives $p^2(f)$. The further integration over f then gives $\overline{y^2}$ and $\overline{p^2}$. The transfer function $\Gamma(\underline{k},\ f)$ is easily obtained [82] , but the integration may prove a stumbling block.

7.5 Coincidence [83] . - A large number of pressure waves (Fig. 22) superpose to form a random pressure field. All orientations and wave lengths appear as the vector $\underline{k}$ varies in direction and length. The frequency f associated with a wave arises from its motion past the observer: e.g., a pressure wave travels in the $\pm\,\underline{k}$ direction with a speed $u = f\lambda = 2\pi f/k$. Consider now possible free running (unforced) flexural waves in the infinite panel. The free waves have characteristic speeds which vary with $\underline{k}$. When a pressure wave and flexural wave match in both speed and wave number (or equivalently, in wave length) the condition is called coincidence (Fig. 23). The result is a very strong excitation of the running flexural wave. Coincidence is a kind of resonance, causing a wave amplitude buildup inversely as the panel damping.

7.6 Running Waves. - Running flexural waves excited by the coincidence effect can show up prominently in panel response [83, 91, 92] . This is demonstrated in Fig. 24 for a finite panel. For this purpose we depart from the description of panel input and output 'signatures' in terms of ($\underline{k}$, f) spectra and employ instead space-time correlations. (The correlations are equally complete descriptions, the pressure correlation being in fact the Fourier transform - in three dimensions - of the pressure spectrum.) In practice the pressures p and p' sensed by microphones flush-mounted in a rigid wall at x and x' (the wall section replaces the flexible panel for this purpose) are electronically multiplied with a relative time delay τ to give $\overline{pp'}$ (x, x', τ): this is the pressure correlation. The corresponding vibration signature of the flexible panel when excited by the $\overline{pp'}$ field is $\overline{yy'}$(x, x', τ). This can be obtained by means of capacitive pickups [93]placed over the panel.

The region of high correlation in the pressure 'signature' has the appearance of an oblique ridge in the plane of X(=x'-x) and τ (Fig. 24). The ridge line (with x fixed) obeys the equation $X = U_c \tau$. It follows that something is moving with a speed U_c. This something is the eddy pattern in the turbulent boundary layer, and its effective average convection speed U_c is of the order of three-fourths the external stream speed. The sinusoidal pressure waves of Fig. 22 therefore move more or less in unisom with a mean speed U_c in the stream direction (there is some spread in the speeds implied by the decay of the ridge line with increasing τ) [84] .

By virtue of the coincidence effect the panel tends to respond with running ripples with a trace speed U_c in the stream direction. Consider the vibration signature in Fig. 24: this describes the panel motion along a line X = x' - x (with x fixed) in the flow direction. The correlation shows an undulating character with strong oblique hills and valleys at a slope U_c; this implies flexural waves travelling with speed U_c. Superposed is a more random pattern which may be regarded as due to reflection of the waves from the boundaries.

7.7 Infinite Panel/Frozen Convected Pattern. - The situation is especially simple if the boundary layer pressure is treated as a "frozen" convected pattern: there is assumed to be no variation in the convection speeds of the individual pressure waves. A pressure wave yawed at an angle φ to the flow direction then moves with the component speed

$$u = U_c \cos \varphi \qquad (27)$$

The frequency f and wave length λ in the frozen pattern are related by

$$f = u/\lambda \quad = uk/2\pi \qquad (28)$$

Thus f is no longer an independent variable in (26).

Turning to the panel behavior, free flexural waves of wave number $\underline{k}$ on an infinite panel can be shown to travel with a speed v proportional to $\overline{k}$,

$$v = kch \tag{29}$$

where c is a constant of the material (a velocity) and h is the panel thickness.

Matching of the pressure and flexural waves - that is, coincidence - occurs when the speeds u and v agree; this give

$$k = \frac{U_c}{ch} \cos\varphi \tag{30}$$

Thus the panel responds selectively to the pressure waves: it resonates at a unique wave number k (or a unique wave length) for a given yaw angle φ given by (30) [83]. This locus of the values of $\underline{k}$ for coincidence is the semicircle shown in Fig. 25.

If the panel damping is η the peak mean square response is $\backsim \eta^{-2}$ and the response is down to one half in a band width $\backsim \eta$. (This is governed by the value of $|\Gamma|^2$ in (26).) We may therefore speak of a coincidence band $\backsim \eta$ in width. The integrated response for $\overline{y^2}$ is proportional to band width times height or η^{-1} [82, 83].

Finite Panel/Fluctuating Convected Pattern. - The semicircular coincidence locus in the k_1, k_2 plane has application to the finite panel as well as to the infinite panel. The regular array of dots (m, n) in Fig. 26 signify the possible resonances of the panel. A particular mode (m, n) is associated with a particular value of wave number $\underline{k} = (k_1, k_2)$,

$$k_1 = m\pi \text{ /panel length}$$

$$k_2 = n\pi \text{ /panel width}$$

where the length is measured in the flow direction. All modes within a band $\pm 1/U_cT$ on either side of coincidence will be strongly excited, the response being down to one-half at the edges [72]. This is due to the allowance for fluctuation or eddy decay in the convected pressure pattern: U_cT is the distance an eddy travels in its lifetime T. The fluctuation can be interpreted crudely as arising from a spread of convection speeds of the components of the pattern. The single speed U_c is in this view replaced by a band which broadens the coincidence line (30) into a coincidence band.

As the band width $2/U_cT$ decreases with increasing eddy lifetime T, the average modal excitation is found to increase in inverse proportion. (A necessary restriction is panel length $>>$ U_cT.) Thus the mean square vibration $\overline{y^2}$ per unit area of panel, which depends on the product of band width and modal excitation, is independent of T. In fact even the smoothed frequency spectrum $\overline{y^2}(f)$ is independent of T. (The smoothed frequency spectrum is obtained experimentally by passage through, say, a 1/3 octave filter, the individual resonance peaks being averaged out.)

In other words, there exists a universal smoothed spectrum of the mean square vibration response, independent of turbulence decay

time T or of panel breadth and width if not too small (many modes must be excited). The spectrum shape in nondimensional form depends solely on the spatial correlation of the boundary layer pressure field.

This rule of the universal spectrum can be extended to the case of a "frozen" convected boundary layer pattern (T = infinity, or zero fluctuation) by going to an infinite panel. This follows from a proviso of the calculations that panel length $>> U_c T$. Presumably a minimum length is necessary to prevent a reverberant build-up of waves reflected from the boundaries. The calculations of [91, 92] appear to show that the travelling flexural waves decay at a rate proportional to 1/T, very much as the pressure eddies driving the waves. This decay simulates the effect of panel damping governed by η.

Except for the last paragraph, the above results were largely brought out in [72] on the basis of a reexamination of the finite panel analysis of [87] . The present writer has similarly reexamined his own infinite-panel/frozen pattern analysis of some years ago [83] . It turns out that the $\overline{y^2}(f)$ spectrum of the infinite panel (already smooth) and the smoothed spectrum of the finite panel are identical for the same pressure input*. This finding confirms the extension of the universal spectrum rule to the infinite panel driven by a frozen convected pressure field. More important, perhaps, it shows that the early work on the problem, long thought to be seriously oversimplified by virtue of the infinite panel/frozen pattern assumptions, gives the correct smoothed spectrum for finite panels in a range of circumstances - and accomplishes this with a very greatly simplified physical and mathematical model.

7.9 Radiation of Sound from Panel Vibration . - The sound radiated from a flexible panel flushmounted in a turbulent flow duct presents a smooth broad band spectrum when measured with a 1/3 octave filter (Fig. 27). The theoretical succession of sound peaks (associated with vibration peaks) is presumably averaged out. The shape roughly resembles that of the input pressure spectrum.

Two different investigations [94, 95] agree on the integrated sound power radiated at low flow speed U: this varies about like U^5 (Fig. 28). At higher speeds, a transition to a $U^{2.3}$ law was found [95] (Fig. 29). A similar transition (but to a U^3 law) was predicted in [83] . The transition appears to be associated with the progressive decrease in the wave lengths for coincidence (see earlier) with increasing flow speed: above a certain speed - the knee in the curve - the shortest wave lengths become shorter than the average correlation length in the driving pressure field. The increasing mismatch reduces the efficiency of excitation.

---

* The methods of [83] were applied to an input correlation of the type used in [87] but with T = ∞ therein, to obtain the corresponding infinite panel/frozen pattern spectrum.

The pressure field correlation length varies essentially as the duct depth. Returning to [94] the depth appears as a second parameter in Fig. 28. We define instead an 'equivalent' boundary layer thickness taken as one half the duct depth. The panel thickness h is varied in still other measurements. The composite results show that for these low speed experiments the sound power radiated from the panels varies approximately like $U^5 \delta^{\frac{1}{2}}/h$.

Figure 30 [91] makes some comparisons of acoustic efficiency, defined as the ratio of radiated sound power to skin friction power (boundary layer) or kinetic energy flux (jet). At the cited low subsonic Mach number of roughly 0.2 the flexible panel is most efficient by over two orders of magnitude. However, the flexible panel noise increases like U^5 diminishing to $U^{2.3}$, the rigid 'panel' noise (rough rotating cylinder)* like U^6 and the jet noise like U^8, so that the ranking will be in inverse order once low supersonic speeds are obtained.

On the theoretical side we have dealt in some detail with the mechanism of the excitation of panel vibration. Space does not permit a comparable discussion of the next step, the more complex theory bridging the gap from vibration to sound generation. The theory is as yet incomplete, and the reader is referred to the references for the details.

A straightforward approach employs simple sources distributed over the panel with local strength proportional to the local normal acceleration [82, 96]. The mean square sound pressure radiated to a point then results as an integral of a weighted space-time correlation of the local panel acceleration. Rather farreaching assumptions have been resorted to simplify the integral.

The running wave approach allows a simple and direct coupling of radiated sound waves [83]. However, the method is limited to the infinite panel and has been applied so far only for a frozen convected boundary layer.

Expressions for the radiation properties of individual modes for finite panels are exploited (in different ways [72, 84]) in a third approach; coupling of the modes is neglected. This method will probably be developed further.

---

* The U^6 law presumably reflects dominant dipole type noise from the surface roughness. For a smooth wall the theoretical behavior is nearer U^8 except for an effect of curvature.

REFERENCES

This list is not an exhaustive bibliography nor is it historically complete despite its length. It does, however, provide an introduction to the rich literature on aircraft noise and related phenomena.

1. Lighthill, M. J., On Sound Generated Aerodynamically I. General Theory, Proc. Roy. Soc. A211, 564-587 (1952).

2. Lighthill, M.J., On Sound Generated Aerodynamically II. Turbulence as a Source of Sound, Proc. Roy. Soc. A222, 1-32 (1954).

3. Lighthill, M.J., The Bakerian Lecture, 1961. Sound Generated Aerodynamically, Proc. Roy Soc. A267, 147-182 (1962).

4. Blokhintsev, D.I., Acoustics of a Nonhomogeneous Moving Medium. In Russian (1946), translated by Natl. Advisory Comm. Aeronaut. as NACA T.M. 1399 (1956).

5. Eldred, K. McK., Noise and Aerodynamic Pressure Fluctuations Anticipated for Space Vehicles. Presented at Second Internat. Conf. on Acoust. Fatigue (sponsored by Air Force Materials Lab.) Dayton, Ohio, (Apr. 29 - May 1, 1964).

6. Howes, W. L., Callaghan, E. E., Coles, W. D., and Mull, H. R., Near Noise Field of a Jet Engine Exhaust. NACA Report 1338 (1957).

7. Harris, C. M. (Ed.), Handbook of Noise Control, Espec. Ch. 33 by H. E. von Gierke, Aircraft Noise Sources, pp. 33 - 30 to 33 - 65, McGraw-Hill, New York (1957).

8. Staff of Langley Research Center. The Supersonic Transport - A Technical Summary. Ch. II, by H. H. Hubbard and D. J. Maglieri "Some Noise Problems of Supersonic Transports", NASA TN D-423 (June 1960).

9. Ribner, H S., The Generation of Sound by Turbulent Jets. Advances in Applied Mechanics, Vol. VIII, Academic Press (N. Y. and London) (to be published).

10. Morse, P. M., Vibration and Sound, McGraw-Hill, 2nd Ed. (1948).

11. Tucker, M., Interaction of a Free Flame Front with A Turbulent Field, NACA Report 1277 (1956).

12. Ribner, H. S., Aerodynamic Sound From Fluid Dilatations - A Theory of Sound from Jets and Other Flows, U. of Toronto, Inst. for Aerospace Studies, UTIA Rep. 86 (AFOSR TN 3430) (1962).

13. Davis, D.D. and Czarnecki, Dynamometer-Stand Investigation of a Group of Mufflers, NACA TN-1838.

14. Lassiter, L.W., Noise from Intermittent Jet Engines and Steady Flow Jet Engines with Rough Burning, NACA TN-2756 (1952).

15. Davis, D.D. and Stokes, Theoretical and Experimental Investigation of Mufflers with Comments on Engine Exhaust Muffler Design, NACA Report No. 1192 (1954).

16. Gutin, L., On the Sound Field of a Rotating Propeller, NACA TM 1195 (1948) (Translated from Physik. Zeitschr. der Sowjet-union, Bd. 9, Heft 1, 1936, pp 57-71).

17. Deming, A.F., Propeller Rotation Noise, Noise Due to Torque and Thrust, NACA TN 747 (1940).

18. Hubbard, H.H., Propeller Noise Charts for Transport Airplanes, NACA TN 2968 (1953).

19. Lamb, H., Hydrodynamics, Sixth Ed., Cambridge Univ. Press, 1932 (reprinted by Dover Publications, New York, 1945), p. 502.

20. Curle, N., The Influence of Solid Boundaries Upon Aerodynamic Sound, Proc. Roy Soc. A231, 505-514 (1955).

21. Garrick, I.E. and Watkins, C.E., A Theoretical Study of the Effect of Forward Speed on the Free-Space Sound Pressure Field Around Propellers, NACA Report 1198 (1954).

22. Van de Vooren, A.I. and Zandbergen, P.J., Noise Field of a Rotating Propeller in Forward Flight, AIAA Jour. 1, 7, 1518 - 1526 (July 1963).

23. Watkins, C.E. and Durling, B.J. - A Method for Calculation of Free-Space Sound Pressures Near a Propeller in Flight Including Considerations of the Chordwise Blade Loading, NACA TN 3809 (1956).

24. Ernsthausen, W., Der rotierenden Tragflugel als Strahlungs-problem, Zeitschr., f. ang. Math and Mech. 31, Heft 1/2, pp. 20-35 (Jan/Feb 1951).

25. Etkin, B., Keefe, R.T. and Korbacher, G.K., Acoustic Radiation from a Stationary Cylinder in a Fluid Stream (Aeolian Tones). J. Acoust. Soc. Amer. 29, No. 1 (Jan. 1957). See also 34, No. 11, 1711-1714 (Nov. 1962) by R.T. Keefe.

26. Hubbard, H. H. and Lassiter, L. W., Some Aspects of the Helicopter Noise Problem, NACA TN 3239 (1954).

27. Greatrex, F. B., By-pass Engine Noise, SAE Preprint 162C (1960), S. A. E. Trans., Vol. 69, p. 312 (1961).

28. Tyler, J. M. and Sofrin, T. G., Axial Flow Compressor Noise Studies, Soc. of Automotive Eng., SAE Paper 345-D (1961).

29. Bragg, S. L., and Bridge, R., Noise from Turbojet Compressors, J. Roy. Aero. Soc., Vol. 68, No. 637, pp. 1 - 10, (Jan. 1964).

30. Griffiths, J. W. R., The Spectrum of Compressor Noise of a Jet Engine, J. Sound and Vibration, Vol. 1 (2), pp. 100-113 (1964).

31. Kramer, M., The Aerodynamic Profile as Acoustic Noise Generator, J. Aero. Sci., 20, No. 4, 280-282; 296 (Apr. 1953).

32. Westervelt, P. J. Aerodynamic Noise: Its Generation and Suppression. General Electric Co., (Schenectady, N. Y.) G.E. Lab Rep. 57GL222 (1957).

33. Sharland, I. J., Sources of Noise in Axial Flow Fans, Univ. of Southampton, Inst. of Sound and Vibr. Res., ISAV Memorandum (Nov. 1963).

34. Lighthill, M. J., Jet Noise, Wright Brothers Lecture, AIAA Jour 1, No. 7, 1507-1517 (July, 1963).

35. Powell, A., On the Generation of Noise by Turbulent Jets, Amer. Soc. Mech. Eng., ASME Paper 59-AV-53 (1959).

36. Ribner, H. S., On the Strength Distribution of Noise Sources Along a Jet, U. of Toronto, Inst. of Aerophysics, Rep. 51 (1958); abridged in J. Acoust. Soc. Amer. 30, 876 (1958).

37. Lilley, G. M., On the Noise from Air Jets, Aeronaut. Res. Counc., ARC 20, 376-N40-FM 2724 (1958).

38. Powell, A., Similarity Considerations of Noise Production from Turbulent Jets, both Static and Moving, Douglas Aircraft Co., Rep. SM-23246 (1958); abridged in J. Acoust. Soc. Amer. 31, 812-813 (1959).

39. Ribner, H. S., On Spectra and Directivity of Jet Noise., J. Acoust. Soc., Amer. 35, No. 4, 614-616 (April 1963).

40. Proudman, I., The Generation of Noise by Isotropic Turbulence, Proc. Roy. Soc. A214, 119-132 (1952).

41. Ffowcs Williams, J.E., The Noise from Turbulence Convected at High Speed. Phil. Trans. Roy. Soc. Lond., Series A, 255, 469-503 (1963)

42. Atvars, J. and Schubert, L.K.O., Preliminary Results of an Investigation of Refraction of Sound by a Jet Flow. Inst. for Aerospace Studies, University of Toronto (June 1964) (unpublished).

43. Eldred, K. et al., Suppression of Jet Noise with Emphasis on the Near Field. Flt. Dynamics Lab., Aeronaut. Systems Div., Air Force Systems Command, Wright-Patterson A.F. Base, Ohio, Report ASD-TDR-62-578 (Feb. 1963).

44. Gottlieb, P., Sound Source Near a Velocity Discontinuity, J. Acoust. Soc. Amer. 32, 1117-1122 (1960).

45. Lassiter, L.W. and Hubbard, H.H., Experimental Studies of Noise from Subsonic Jets in Still Air, NACA TN 2757 (1952).

46. Phillips, O.M., On the Generation of Sound by Supersonic Turbulent Shear Layers, J. Fluid Mech. 9, 1-28 (1960).

47. Greatrex, F.B., Noise Suppressors for Avon and Conway Engines, Amer. Soc. Mech. Engrs. Paper No. 59-AV-49 (1959).

48. Lee, Robert et al, Research Investigation of the Generation and Suppression of Jet Noise, General Electric Co., Flt. Propuls. Lab. Dept. (Cincinnati), prepared under Navy Bu. Weapons Contract No. as 59-6160-c (1961).

49. Busemann, A., The Relation Between Minimizing Drag and Noise at Supersonic Speeds. Proc. of Conf. on High Speed Aeronautics, Polytech. Inst. of Brooklyn, Jan. 20-22, 1955 (Edwards Bros., U.S.A.)

50. Randall, D.G., Methods for Estimating Distributions and Intensities of Sonic Bangs. R A.E. Rep. and Mem. No. 3113 (August 1957).

51. Lyster, H.N.C., A Review of Theoretical and Experimental Information Relating to the Sonic Boom. National Research Council (Canada), Aeronautical Report LR-313 (September 1961).

52. Warren, C.H.E., Sonic Bangs: A Qualitative Explanation. R.A.E. TN Aero. 2192 (1952).

53. Lilley, G.M., Westley, R., Yates, A.H. and Busing, J.R. Some Aspects of Noise from Supersonic Aircraft. Jour. Roy. Aero. Soc. (June. 1953).

54. Cabannes, H., Influence des Accelarations sur la Courbure des Chocs.. La Recherche Aeronautique, No. 39, pp. 3-13 (May-June, 1954).

55. Rao, P. S., Supersonic Bangs, Part I., Aero. Quart. 7, Part I, 21-44 (February 1956).

56. Rao, P. S., Supersonic Bangs, Part II, Aero. Quart 7, Part II, 135-155 (May 1956).

57. Warren, C.H.E. and Randall, D.G., The Theory of Sonic Bangs, Progress in Aeronautical Sciences, Vol. I, pp. 238-274 (Pergamon Press, 1961).

58. Friedman, M.P., Kane, E.J., and Sigalla, A., Effects of Atmosphere and Aircraft Motion on the Location and Intensity of a Sonic Boom. AIAA Jour., 1, No. 6, 1327-1335 (June 1963).

59. Whitham, G.B., The Flow Pattern of a Supersonic Projectile. Comm. on Pure and Appl. Math., V, pp. 301-348 (Aug. 1952).

60. DuMond, J.W.M., Cohen, E.R., Panofsky, W.K H., and Deeds, E., A Determination of the Wave Forms and Laws of Propagation and Dissipation of Ballistic Shock Waves. J. Acoust. Soc. Amer., 18, No. 1, pp. 97-118 (July 1946).

61. Maglieri, D.J., Ritchie, V.S., and Bryant, J.F., Jr., In-Flight Shock-Wave Pressure Measurements Above and Below a Bomber Airplane at Mach Numbers from 1.42 to 1.69. NASA TN D-1968 (Oct. 1963).

62. Jones, R.T., Theory of Wing-Body Drag at Supersonic Speeds. NACA Report 1284 (1956).

63. Walkden, F., The Shock Pattern of a Wing-Body Combination Far from the Flight Path. Aeronaut. Quart. IX, Pt. 2, 164-194 (May 1958).

64. Morris, J., An Investigation of Lifting Effects on the Intensity of Sonic Booms. Jour. R.A.S. 64, No. 598, pp. 610-616 (Oct. 1960).

65. Randall, D.G., The Effect of Incidence on Sonic Bang Intensities. R.A.E. Tech. Note. No. Structures 332 (Apr. 1963).

66. Bishop, D.E., Cruise Flight Noise Levels in a Turbojet Transport Airplane. Noise Control 7, No. 2 (Mar - Apr. 1962).

67. Phillips, O.M., Surface Noise from a Plane Turbulent Boundary Layer. A.R.C. Rep. No. 16 963 (1954).

68. Powell, A., Aerodynamic Noise and the Plane Boundary. J. Acoust. Soc. Amer. 32, No. 8, 982-990 (1960).

69. Hodgson, T.H., Pressure Fluctuations in Shear Flow Turbulence Ph.D. Thesis, College of Aeronautics (Cranfield)Note No. 129(1962).

70. Lilley, G.M., Wall Pressure Fluctuations Under Turbulent Boundary Layers at Subsonic and Supersonic Speeds. College of Aeronautics (Cranfield). Note No. 140 (1963).

71. Ffowcs Williams, J.E., Thoughts on the Problem of Aerodynamic Noise Sources Near Solid Boundaries. National Physical Laboratories. N.P.L. Aero. Rep. 1055 (1963).

72. Ffowcs Williams, J.E. and Lyon, R.H., The Sound Radiated from Turbulent Flows Near Flexible Boundaries. Bolt Beranek and Newman Inc. Rept. No. 1054 (submitted to Office of Naval Research) (Aug. 1963).

73. Meecham, W.C., Surface and Volume Sound from Boundary Layers. University of Minnesota, Dept. of Aero. and Eng. Mechanics Rept. (1964).

74. Willmarth, W.W., Space-Time Correlations and Spectra of Wall Pressure in a Turbulent Boundary Layer. NASA Memo 3-17-59W (1959).

75. Serafini, J.S., Wall-Pressure Fluctuations and Pressure-Velocity Correlations in a Turbulent Boundary Layer. NASA TR R-165. (Dec. 1963).

76. Bull, M.K. Wilby, J.F., and Blackman, D.R., Wall Pressure Fluctuations in Boundary Layer Flow and Response of Simple Structures to Random Pressure Fields. Univ. of Southampton, Dept. of Aero. and Astro., A.A.S.U. Rep. No. 243 (July 1963).

77. Kraichnan, R.H., Pressure Fluctuations in Turbulent Flow over a Flat Plate. J. Acoust. Soc. Am. 28, 1048 (1956).

78. Willmarth, W.W., Wall Pressure Fluctuations in a Turbulent Boundary Layer. J. Acoust. Soc. Am. 28, 1048 (1956).

79. Kistler, A.L., Surface Pressure Fluctuations Produced by Attached and Separated Supersonic Boundary Layers. Advis. Grp. Aero. Res. & Develop, NATO, AGARD Report 458 (Apr. 1963).

80. Ribner, H.S., The Effects of Boundary Layer Noise and Oscillating Shock Waves on Skin Panels. II - Skin Stresses from Oscillating Shock Waves. Unpublished report to Avro Aircraft Co., Canada (1957).

81. Ungar, E.E., Wright Air Development Div., Air. Res. and Develop. Command, USAF, WADD Tech. Rep. No. 60-445 (1960).

82. Corcos, G.M. and Liepmann, H.W., On the Transmission Through a Fuselage of Boundary Layer Noise. Douglas Aircraft Company, Santa Monica Division, Rep. SM-19570 (Dec. 1955).

83. Ribner, H.S., Boundary-Layer-Induced Noise in the Interior of Aircraft. University of Toronto, Institute of Aerophysics, UTIA Rep. 37 (Apr. 1956).

84. Kraichnan, R.H., Noise Transmission from Boundary Layer Pressure Fluctuations. Jour. of the Acoustical Society of America, Vol. 29, No. 1 (Jan. 1957).

85. Lyon, R.H., Response of Strings to Random Noise Fields., J. Acoust. Soc. Amer. 28, 3, 391-398 (1956); see also 33, 11, 1606-1609(1961).

86. Powell, A., On Structural Vibration Excited by Random Pressures with Reference to Structural Fatigue and Boundary Layer Noise. Douglas Aircraft Co., Santa Monica Div., Rep. No. SM-22795 (1957).

87. Dyer, I., Response of Plates to a Decaying and Convecting Random Pressure Field. J. Acoust. Soc. Amer. 31, 7, 922-928 (1959).

88. Tack, D.H., and Lambert, R.F., Response of Bars and Plates to Boundary Layer Turbulence. Jour. of the Aerospace Sciences, Vol. 29, No. 3 (Mar. 1962).

89. Lin, Y.K., Nonstationary Response of Continuous Structures to Random Loading, J. Acoust. Soc. Amer. 35, No. 2, 222-227 (Feb. 1963).

90. Miles, J.W., On Structural Fatigue Under Random Loading, J. Aero. Sci. 21, No. 11, pp. 753-762 (Nov. 1954).

91. Baroudi, M.Y., Ludwig, G.R. and Ribner, H.S. An Experimental Investigation of Turbulence-Excited Panel Vibration and Noise (Boundary Layer Noise). Advis. Grp. Aero Res. & Develop. (AGARD), NATO, Rep. 465 (Apr. 1963).

92. Baroudi, M.Y., Turbulence-Induced Panel Vibration. Inst. for Aerospace Studies, Univ. of Toronto, UTIAS Rep. 98 (April, 1964).

93. Shattuck, R.D., Capacitance-Type Displacement Probe. J. Acoust. Soc. Amer., 31, No. 10 (Oct. 1959).

94. Ludwig, G.R., An Experimental Investigation of the Sound Generated by Thin Steel Panels Excited by Turbulent Flow (Boundary Layer Noise.). Inst. of Aerophysics, Univ. of Toronto, UTIA Rep. 87(Nov. 1962).

95. Maestrello, L., Test Results from the Boundary Layer Facility (Noise Radiated by the Panel)- Vol. I. The Boeing Co., Transport Div., Doc. No. D6-9944 - Vol. I (Feb. 1964).

96. Strasberg, M., Response of Plates and Membranes to Pressure Fluctuations of a Turbulent Boundary Layer. J. Acoust. Soc. Amer. 30, No. 7, 680 (A) (July 1958).

TABLE I

TYPICAL FLUCTUATING PRESSURE LEVELS ON VEHICLE SURFACE FROM VARIOUS CAUSES
(estimated)

		db re. 0002 dynes/cm^2		
OSCILLATING SHOCKS	to	177	L	[5]
ROCKET	to	172	L	[5]
SEPARATED FLOW	to	168	L	[5]
TURBOJET	to	155	T	[6]
PROPELLER	to	150	T	[7]
BOUNDARY LAYER	to	144	SST	[8]
	to	137	T	

L Launch vehicle at q = 800 p. s. f.

T Subsonic transport airplane

SST Supersonic transport airplane,
M = 2.3 to 4. 0, 60 to 70 thousand ft. altitude.

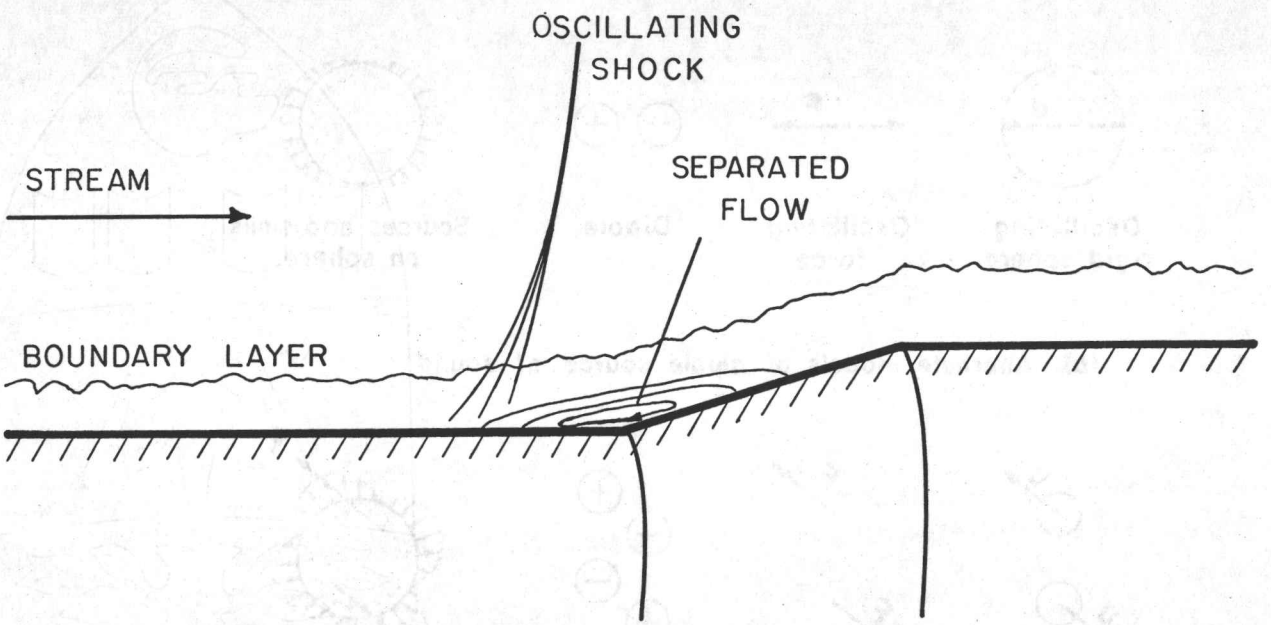

FIGURE I. SOURCES OF NOISE AND VIBRATION AT A ROCKET BOOSTER JUNCTION.

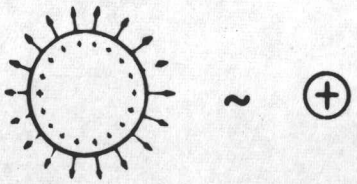

(a) Pulsating sphere as model of simple source of sound

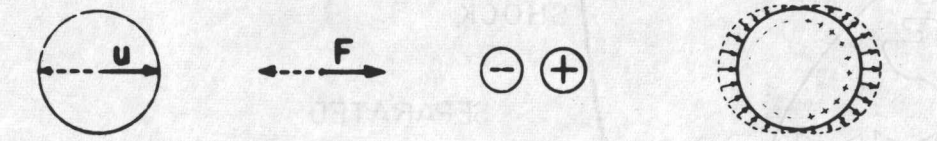

Oscillating rigid sphere | Oscillating force | Dipole | Sources and sinks on sphere

(b) Alternate models of dipole source of sound

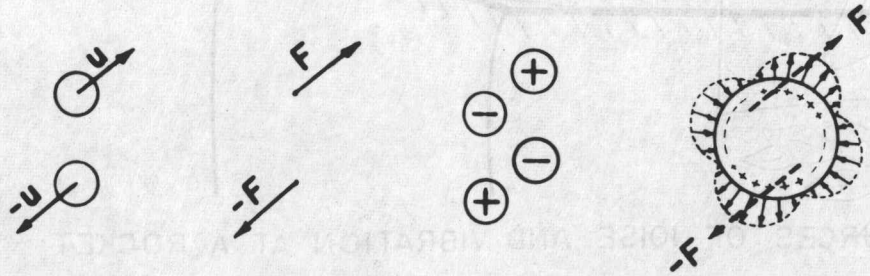

Rigid spheres | Force pair (stress) | Dipole pair | Deforming sphere

(c) Alternate models of oblique quadrupole source of sound

FIG. 2. ELEMENTARY SOURCES OF SOUND. [9].

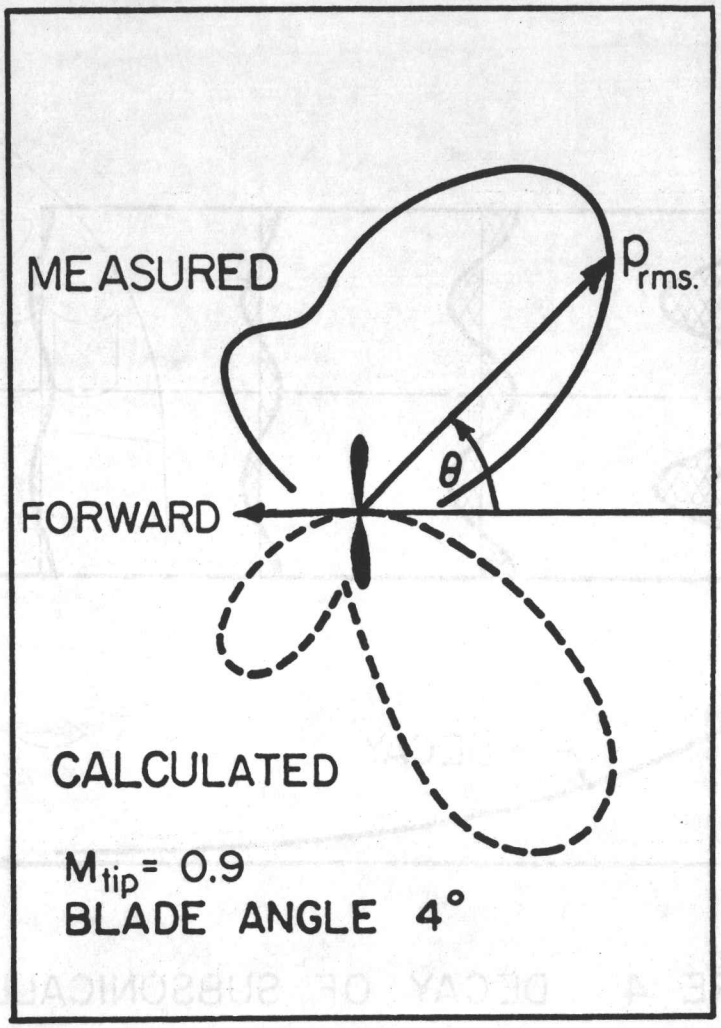

FIGURE 3. MEASURED AND CALCULATED SOUND FIELD OF FUNDAMENTAL TONE OF A MODEL PROPELLER (Adapted from [7], after Ernsthausen [24]).

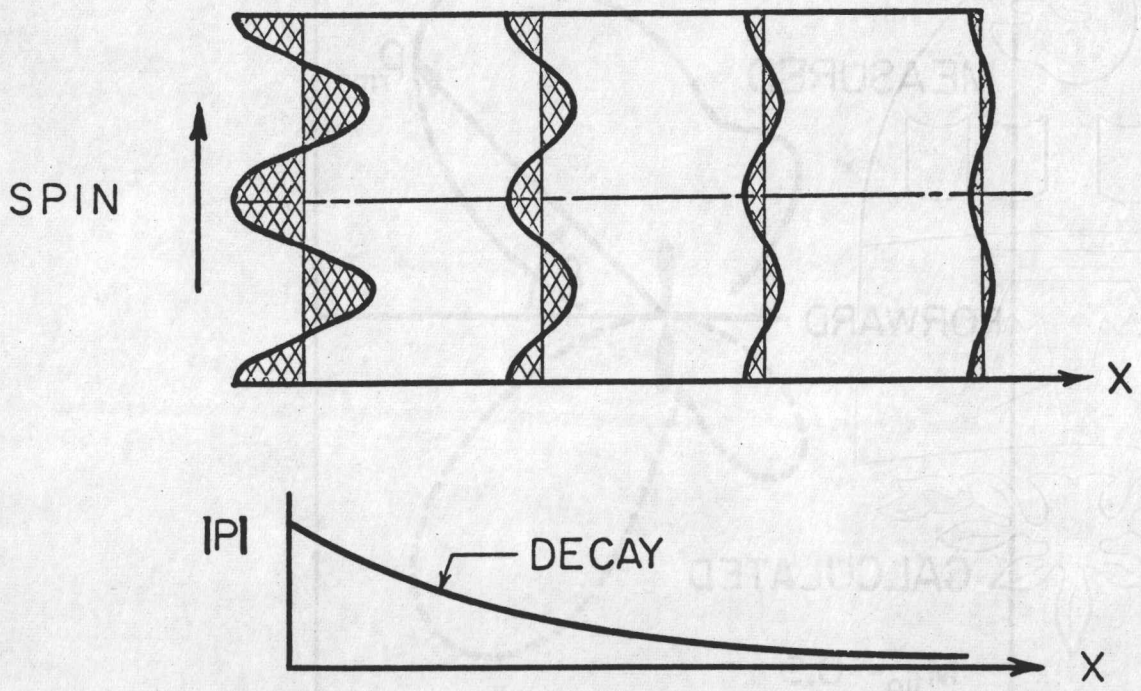

FIGURE 4. DECAY OF SUBSONICALLY SPINNING PRESSURE MODE ALONG ANNULAR DUCT (DEVELOPED VIEW) (AFTER [28]).

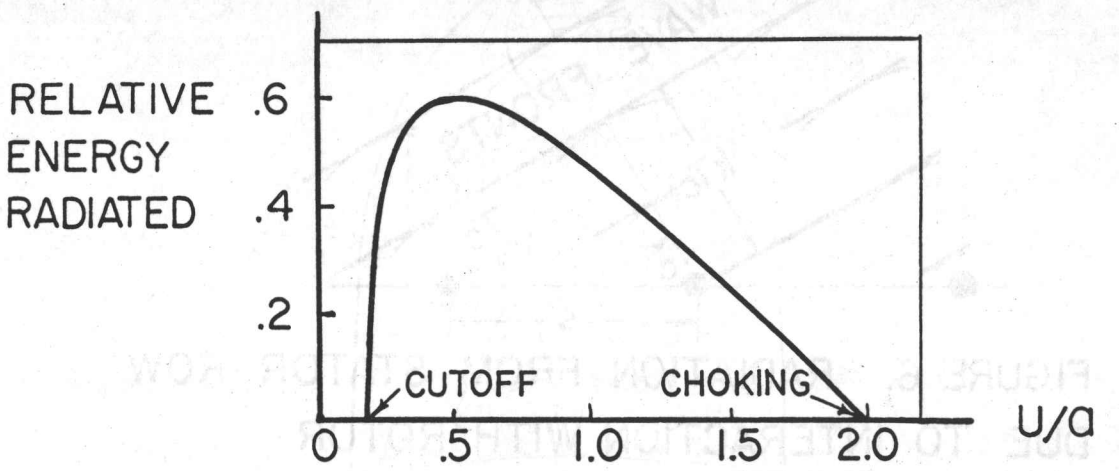

FIGURE 5. RADIATION BEHAVIOR OF TYPICAL STATOR ROW (19 stators, 23 rotors, 45° stagger; After [29]).

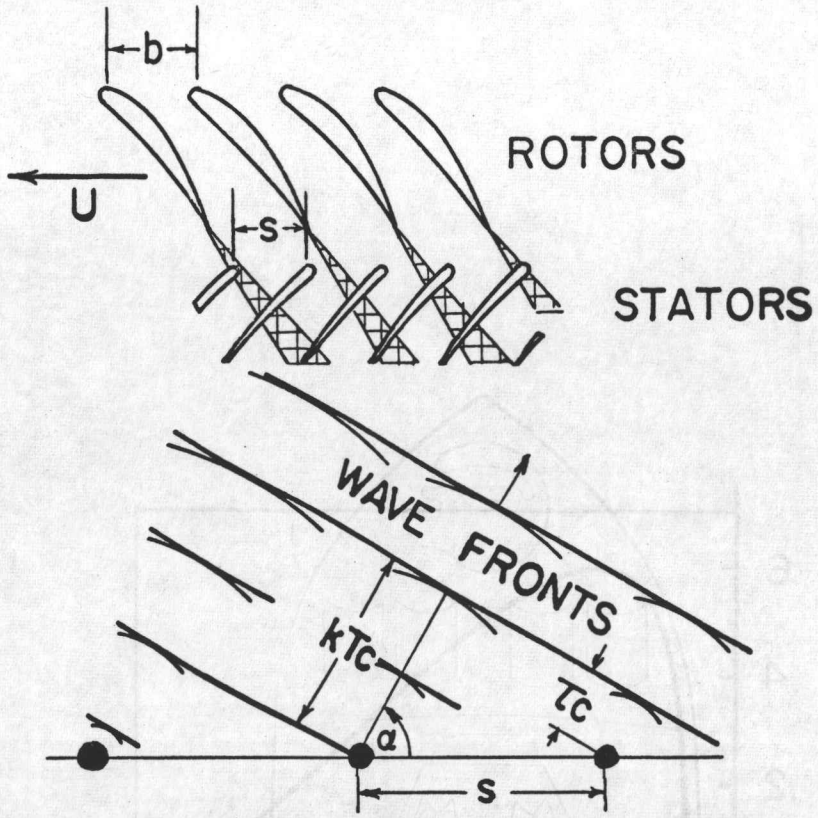

FIGURE 6. RADIATION FROM STATOR ROW DUE TO INTERACTION WITH ROTOR

(Adapted from [29]).

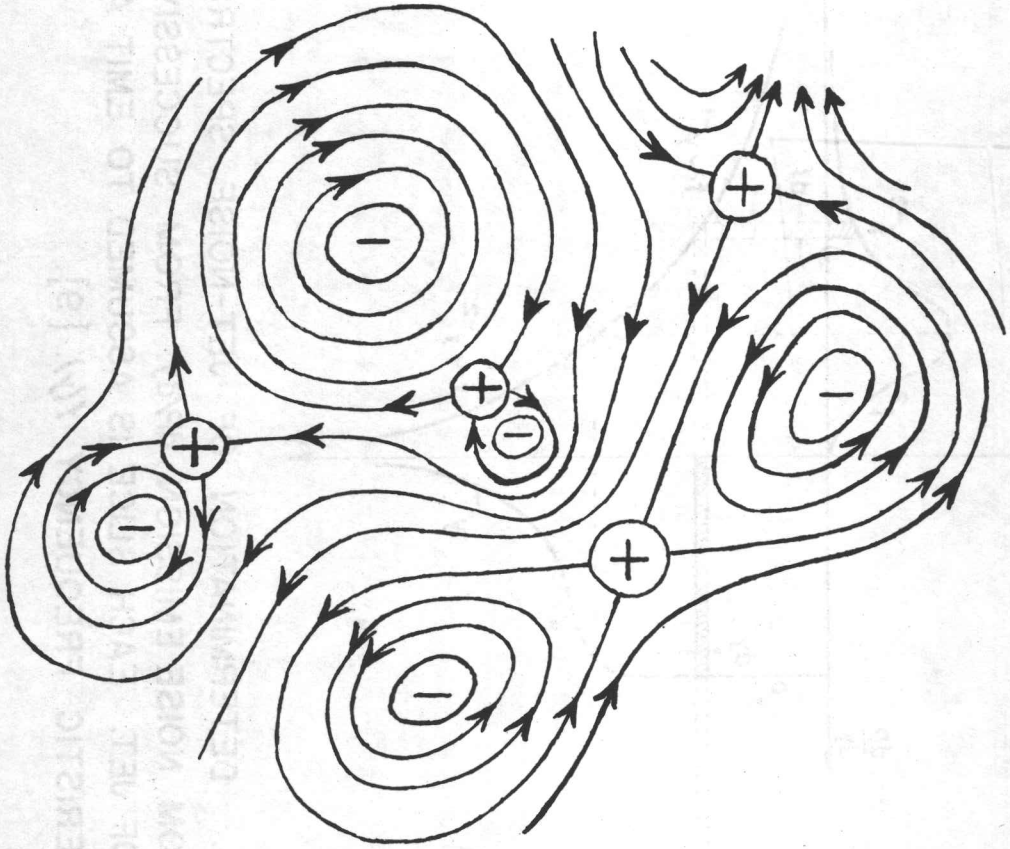

FIGURE 7. POSITIVE ⊕ AND NEGATIVE ⊖ DILATATIONS IN AN EDDYING FLOW. THE LOCAL PRESSURE FIELD (ESSENTIALLY 'PSEUDOSOUND') HAS THE OPPOSITE SIGN. [12]

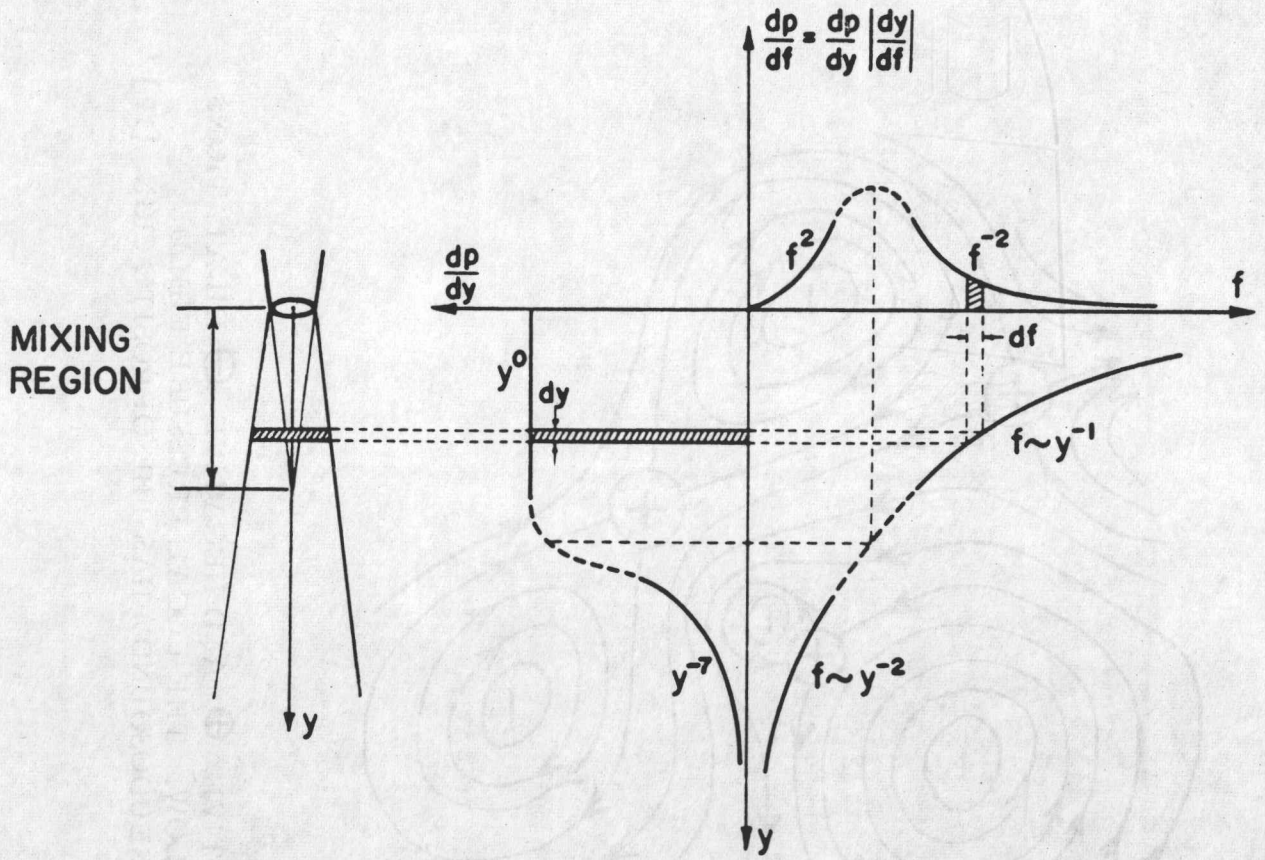

FIGURE 8. DETERMINATION OF JET-NOISE SPECTRUM dP/df FROM NOISE EMISSION dP/dy FROM SUCCESSIVE SLICES OF JET. EACH SLICE IS ASSUMED TO EMIT A CHARACTERISTIC FREQUENCY *f(y)*. [9].

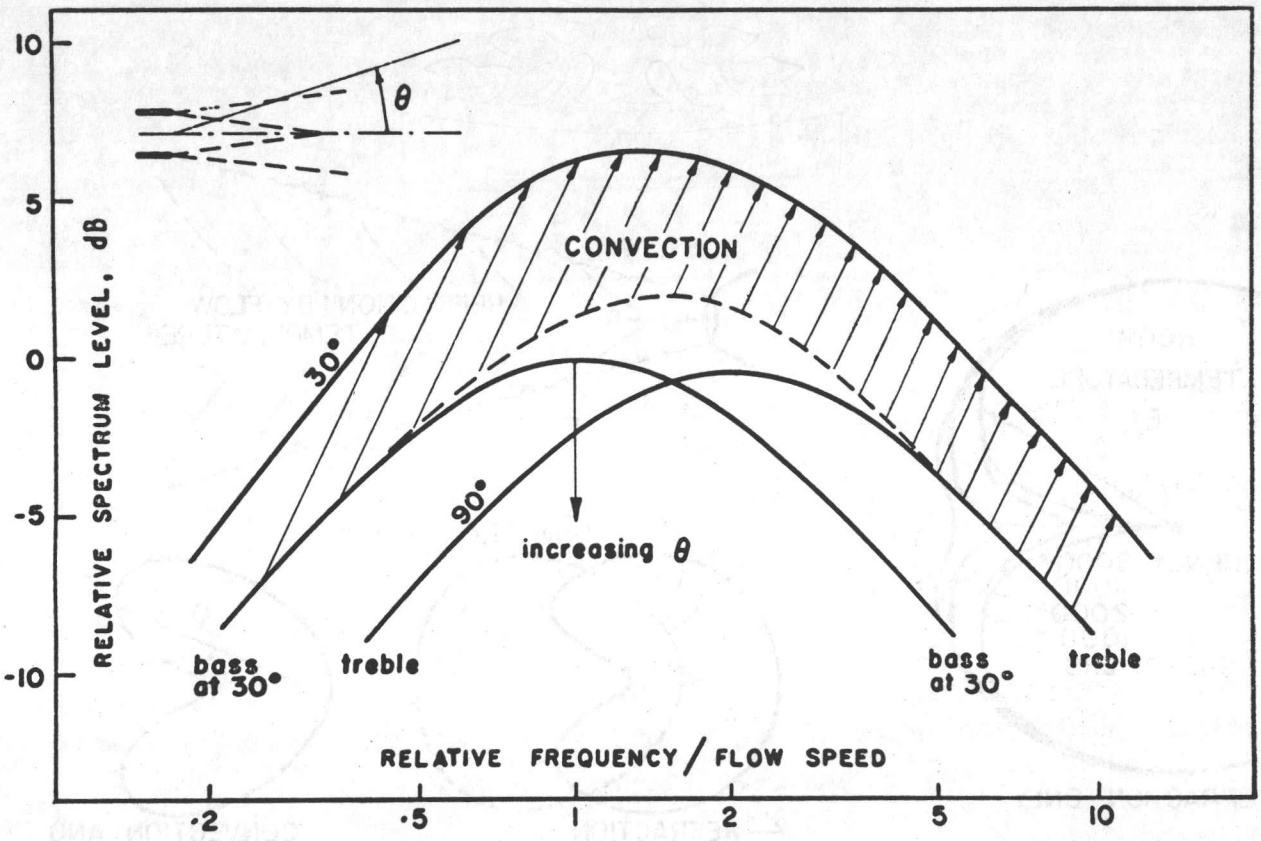

FIGURE 9. VARIATION OF THEORETICAL IDEALIZED JET NOISE SPECTRUM WITH EMISSION ANGLE θ. RELATIVE HEIGHTS OF "BASS" AND "TREBLE" WITHOUT ALLOWANCE FOR CONVECTION ARE IN APPROXIMATE RATIO $2\cos^4\theta$ TO 1. CONVECTIVE AMPLIFICATION COUPLED WITH DOPPLER SHIFT YIELDS FINAL (UPPER) 30° CURVE. [39].

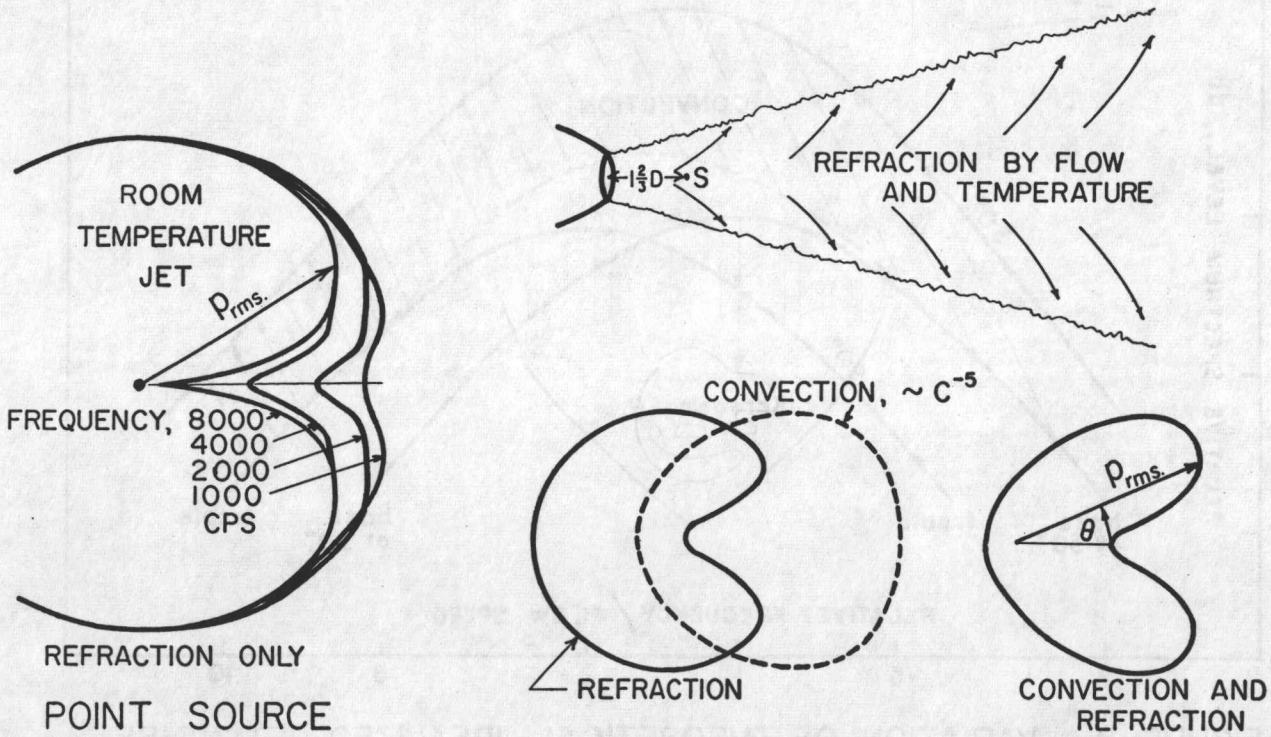

FIG. 10. REFRACTION AND CONVECTION EFFECTS ON DIRECTIVITY. ($(1 + \cos^4\theta)$ FACTOR OMITTED FROM THEORY.)

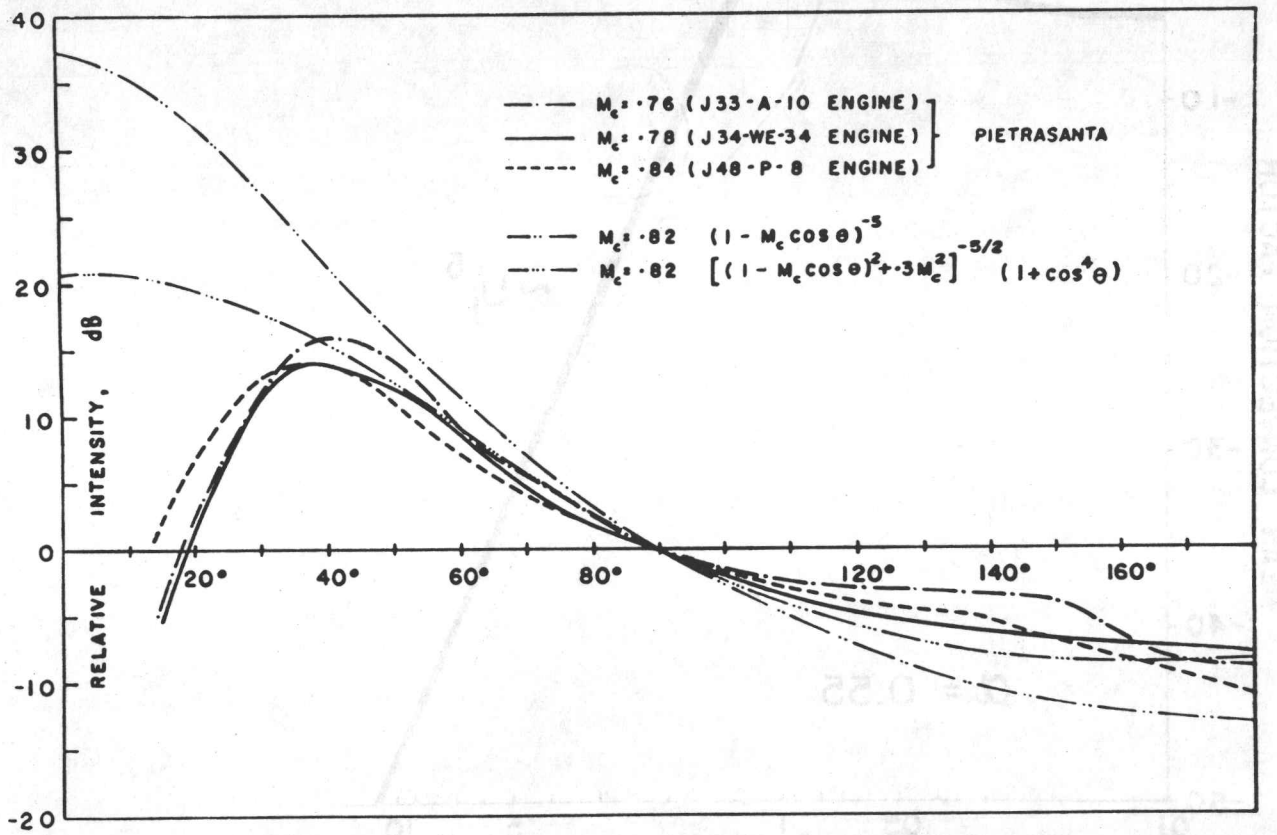

FIG. 11. RELATIVE INTENSITY OF TURBOJET NOISE VERSUS ANGLE θ FROM FLOW DIRECTION (REFERRED TO ZERO db AT 90°). [39].

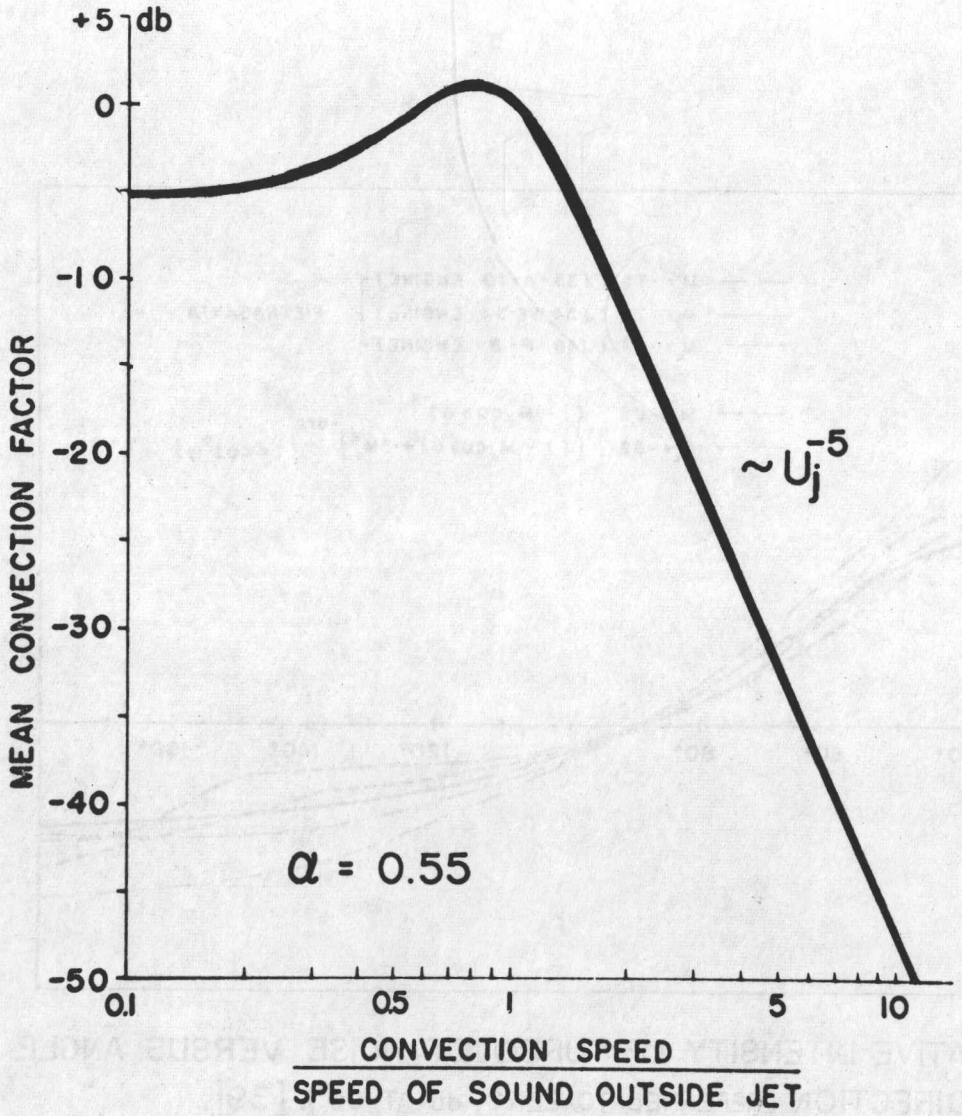

FIG. 12. DIRECTIONAL AVERAGE OF CONVECTION FACTOR, $(C^{-5})_{AV}$, IN *db* RELATIVE TO VALUE AT $M_c = 1$. THIS MULTIPLIES LOW-SPEED POWER LAW (E.G. U_j^{8}). [9].

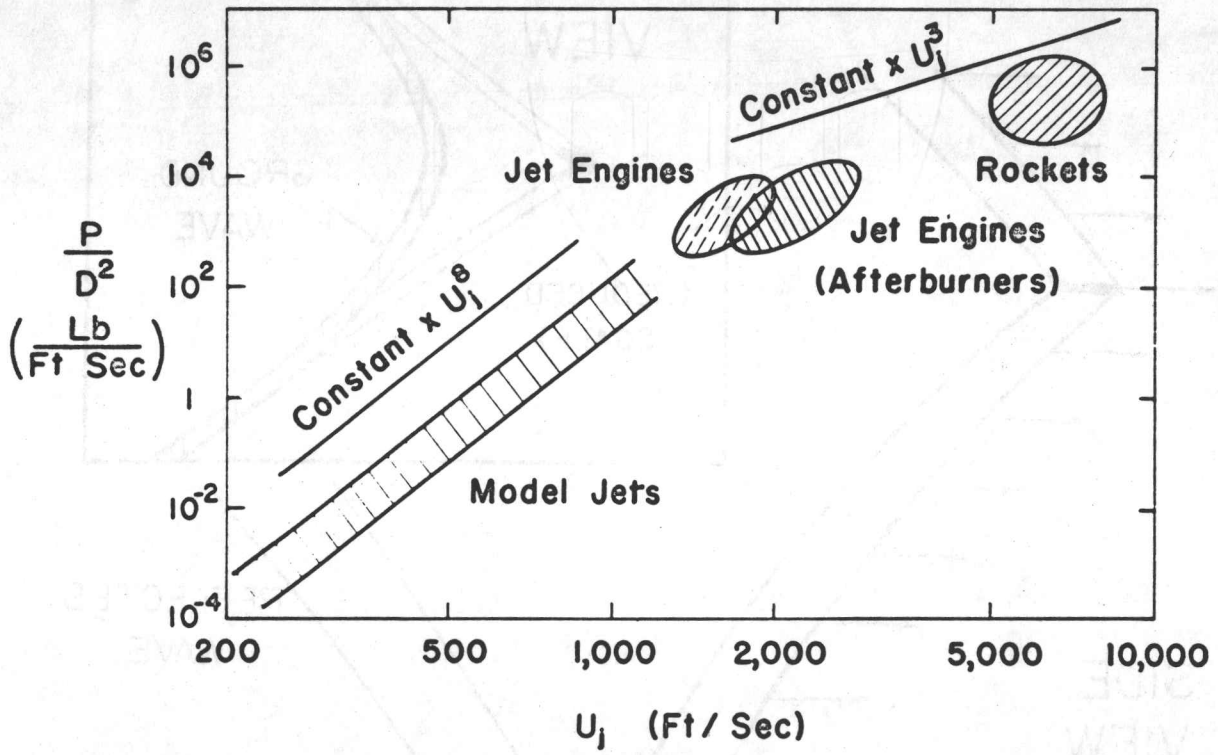

FIG. 13. NOISE POWER VS. JET SPEED, SHOWING TRANSITION FROM $\sim U_j^8$ TO $\sim U_j^3$, APPROXIMATELY, WHEN CONVECTION SPEED $U_j/2$ EXCEEDS THE SPEED OF SOUND (REPRODUCED FROM POWELL [35]).

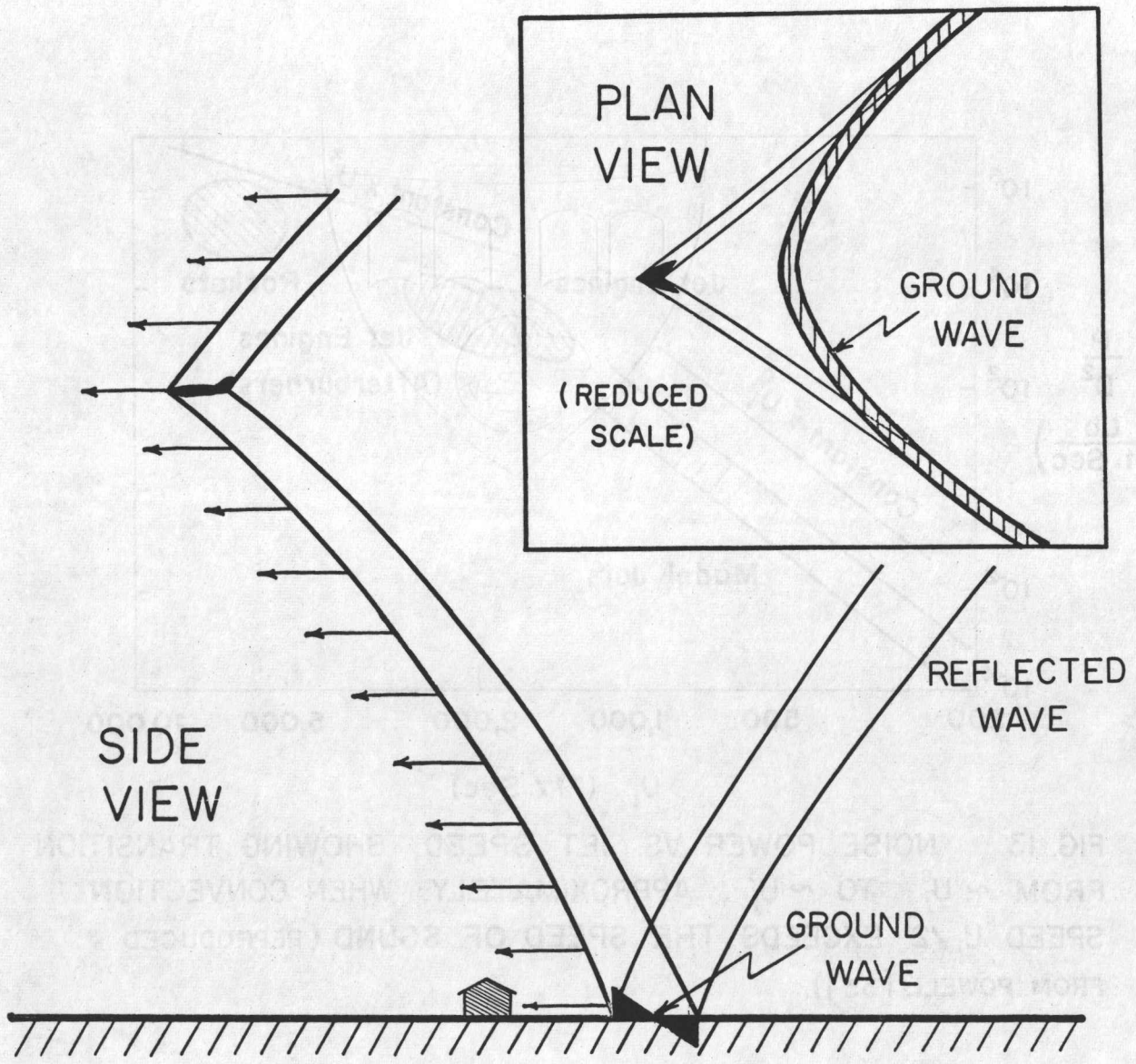

FIGURE 14. SONIC BOOM.

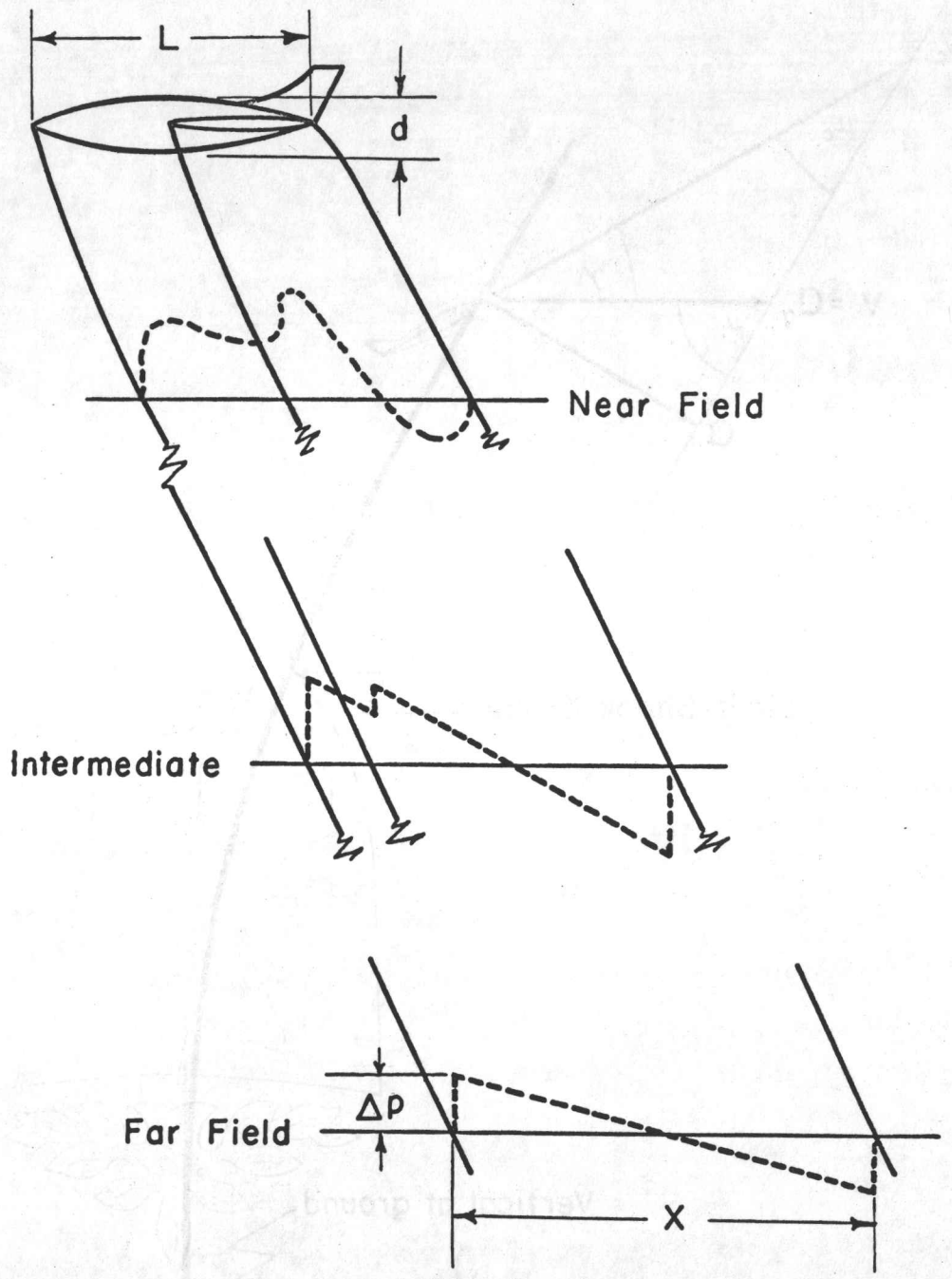

FIG. 15. EVOLUTION OF N-WAVE. (AFTER MORRIS [64]).

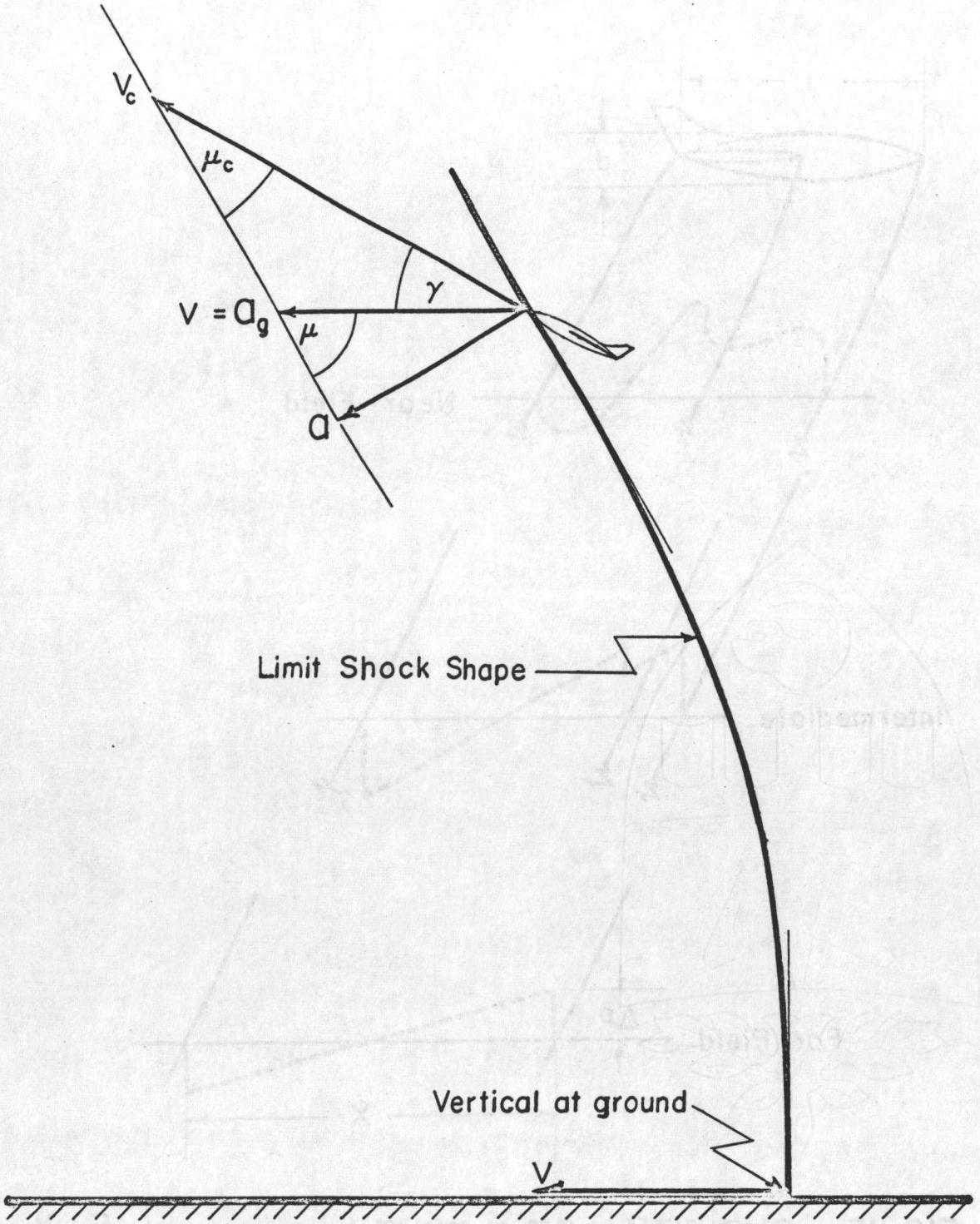

FIG. 16. CONSTRUCTION TO OBTAIN CUT-OFF MACH NUMBER. (AFTER LYSTER [51]).

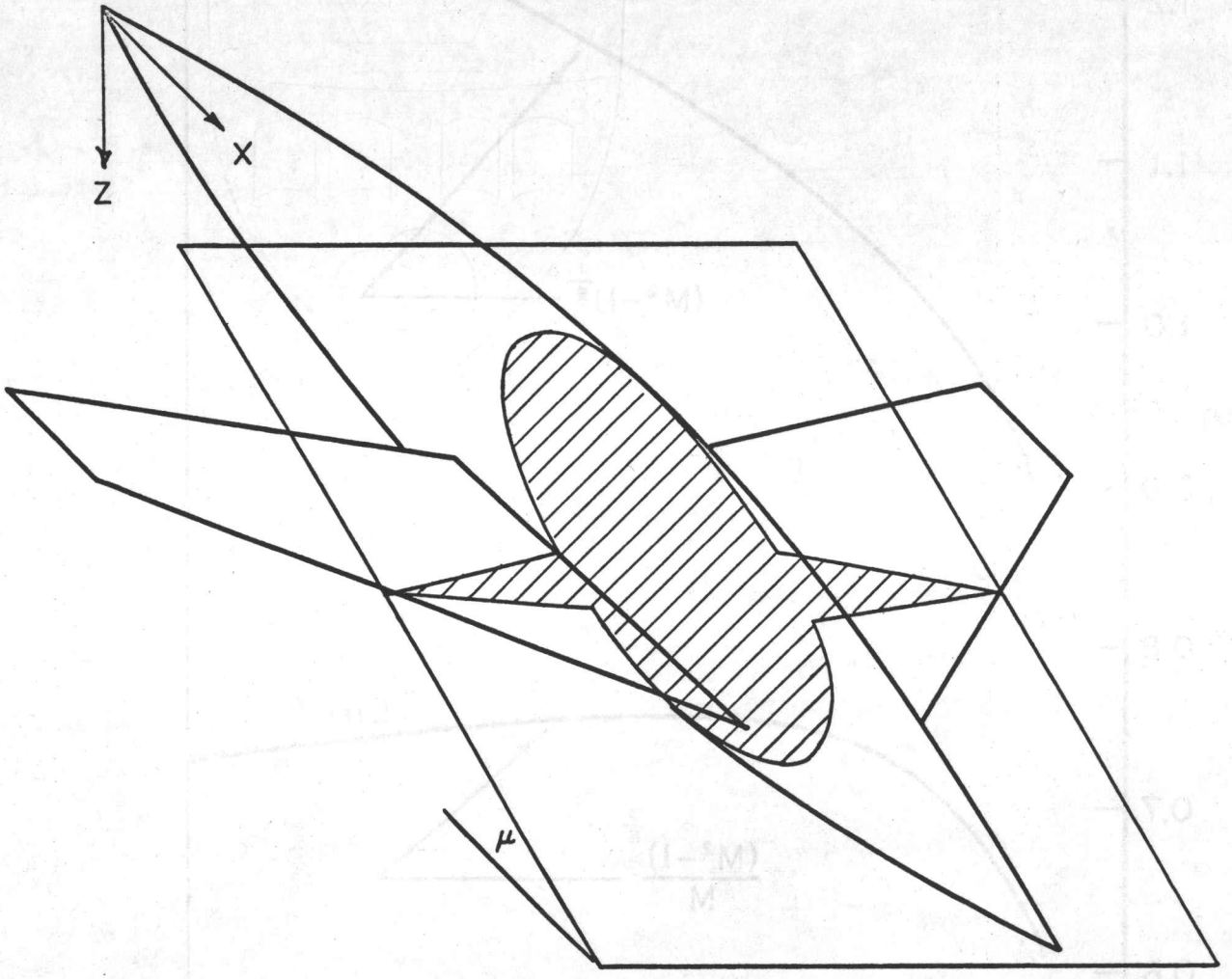

FIG. 17. CONSTRUCTION FOR USE OF SUPERSONIC AREA RULE. (AFTER MORRIS [64]).

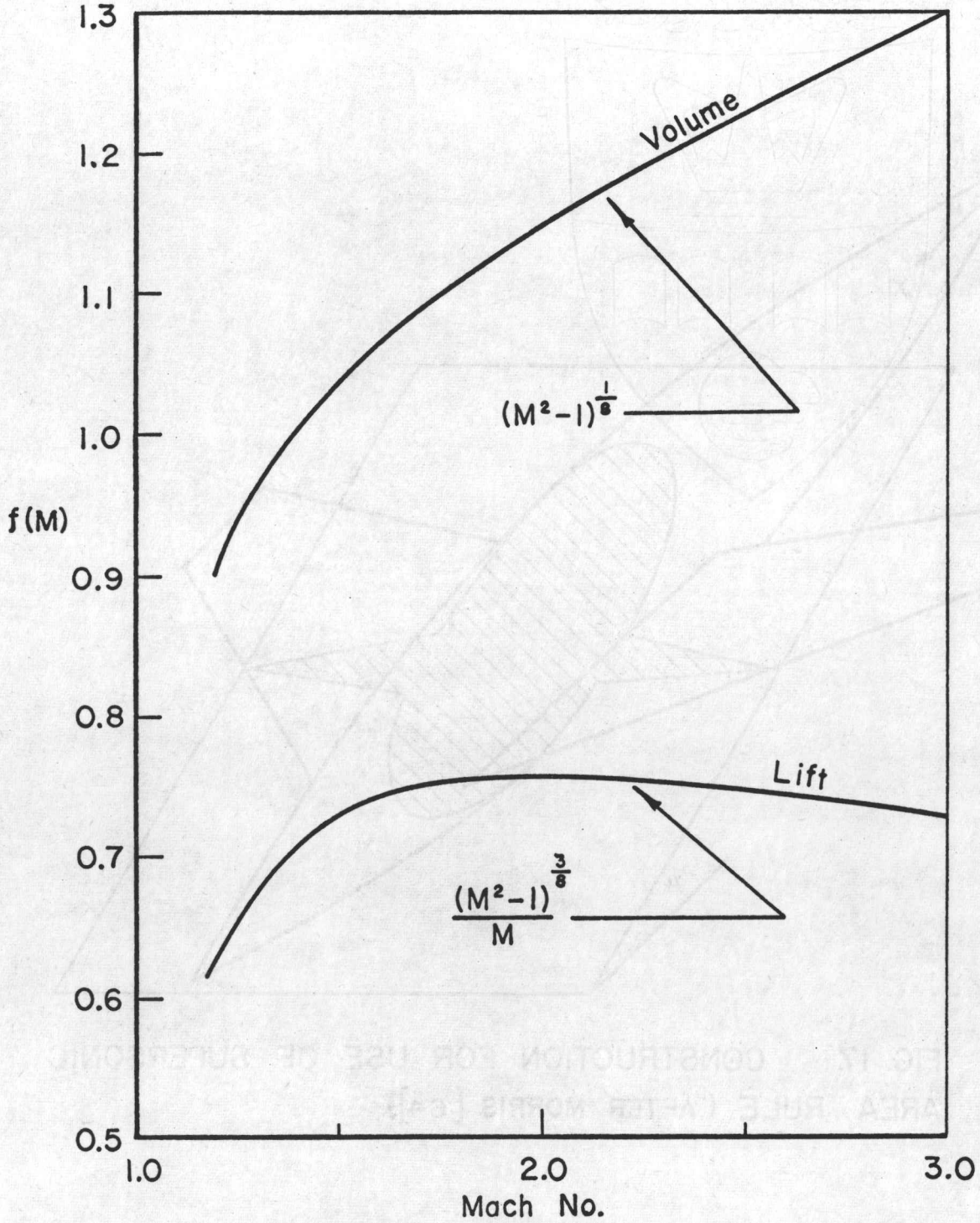

FIG. 18. RELATIVE BOOM INTENSITY VS. MACH NUMBER. (AFTER MORRIS [64]).

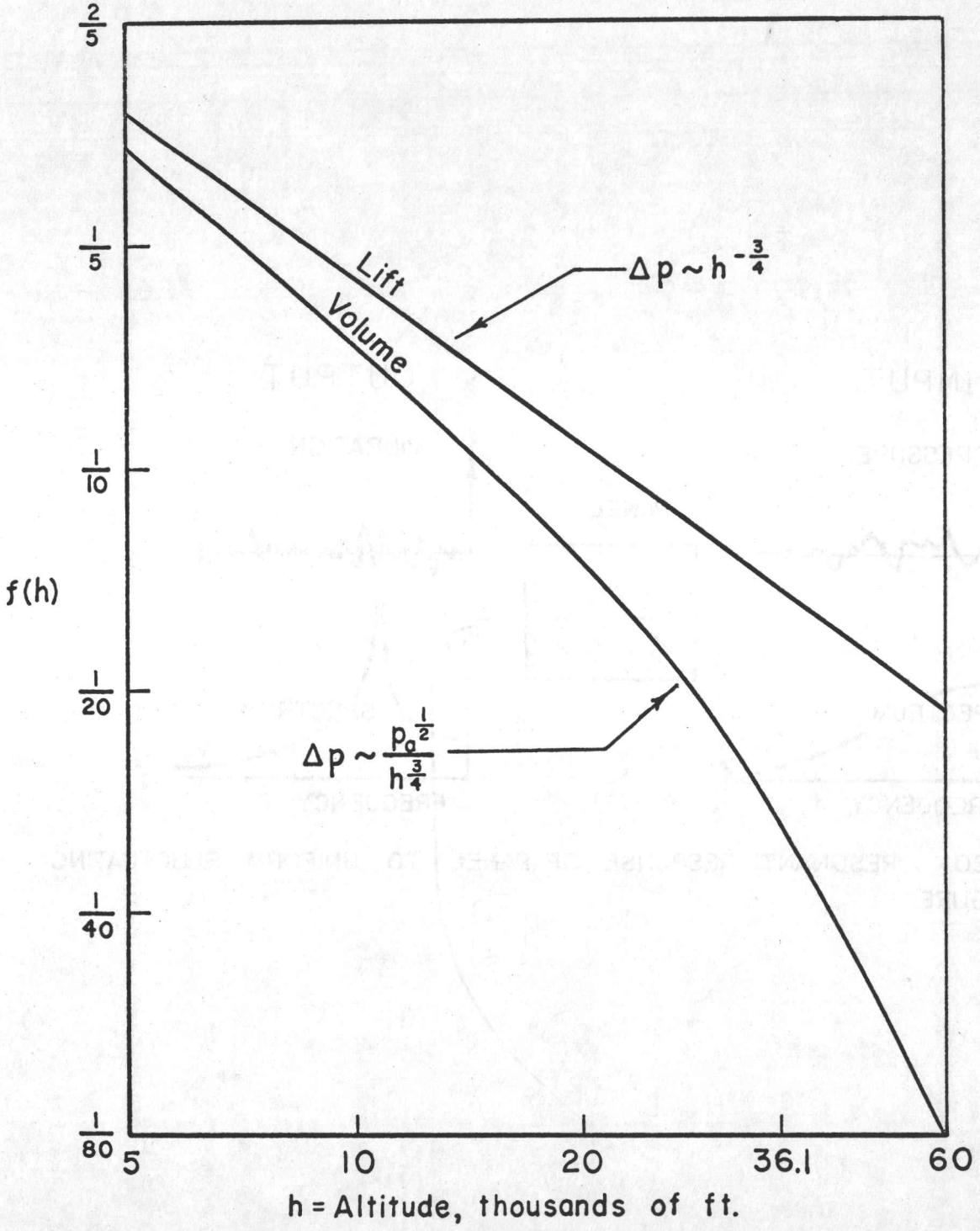

FIG. 19. RELATIVE BOOM INTENSITY VS. ALTITUDE (AFTER LYSTER [51]).

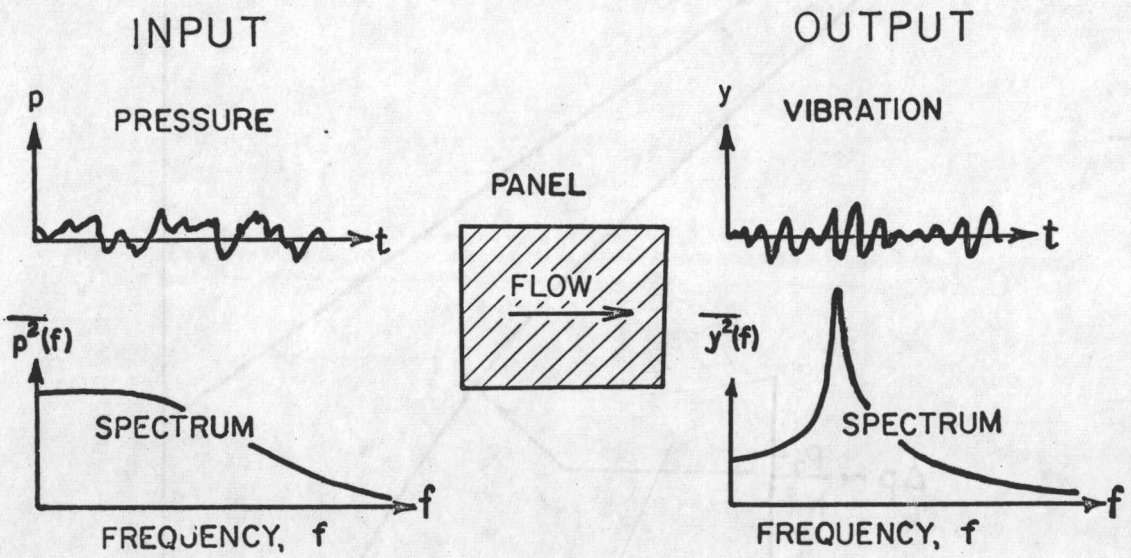

FIG. 20. RESONANT RESPONSE OF PANEL TO UNIFORM FLUCTUATING PRESSURE.

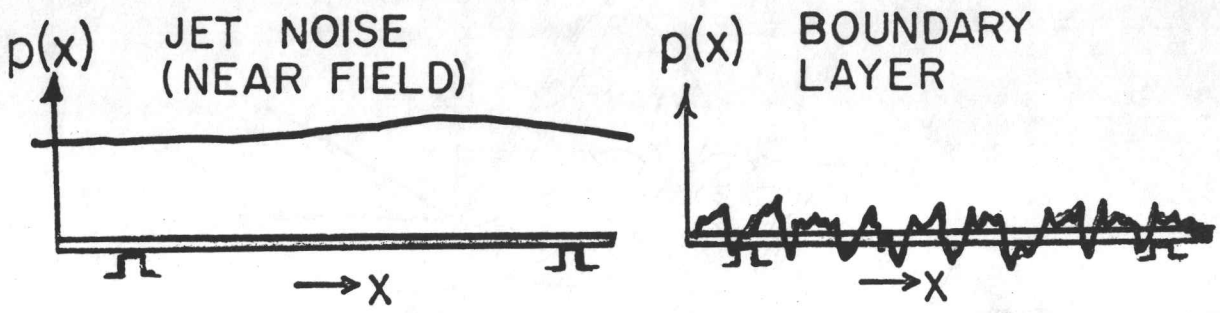

FIGURE 21. PRESSURE FIELD ON FUSELAGE SKIN {Adapted from [82]}.

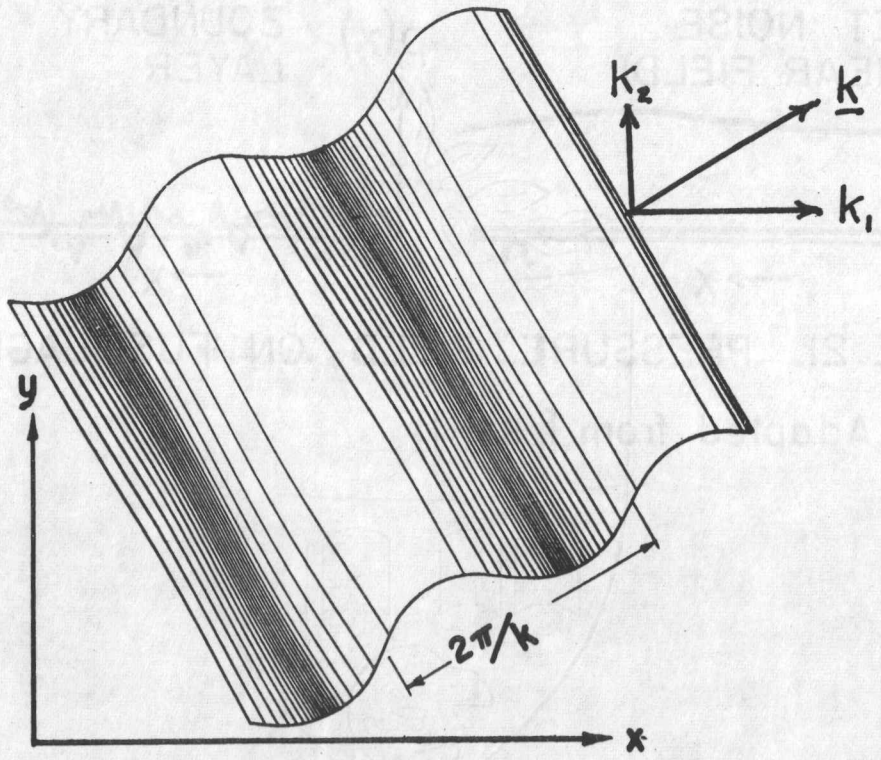

FIG. 22 TYPICAL PRESSURE WAVE IN DECOMPOSITION OF RANDOM SPATIAL PATTERN.

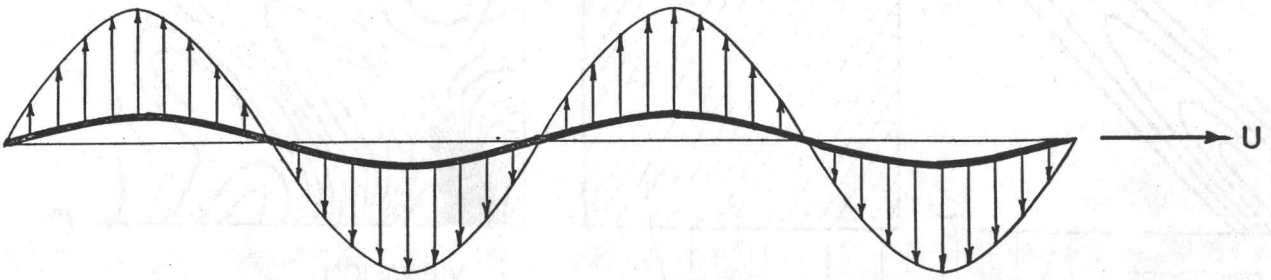

FIGURE 23. COINCIDENCE: WAVELENGTHS OF FORCING PRESSURE WAVE AND FREE-RUNNING FLEXURAL WAVE MATCH FOR THE SAME SPEED.[83].

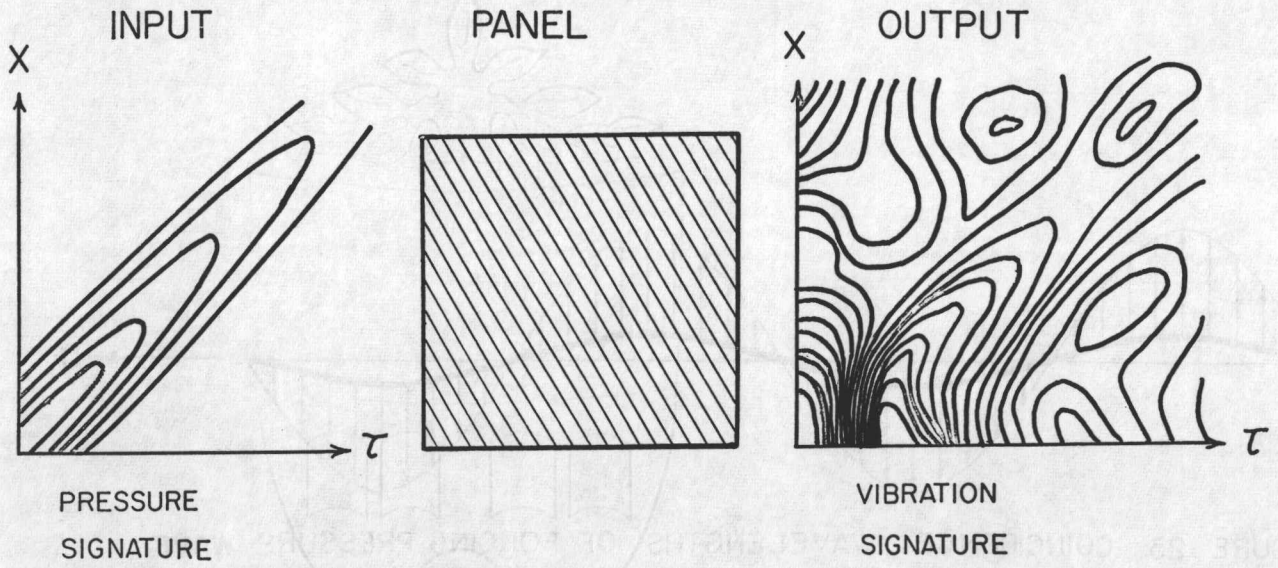

FIGURE 24. CONVECTED PRESSURE FIELD (DUE TO BOUNDARY LAYER) EXCITES RUNNING WAVES. (ADAPTED FROM [91]).

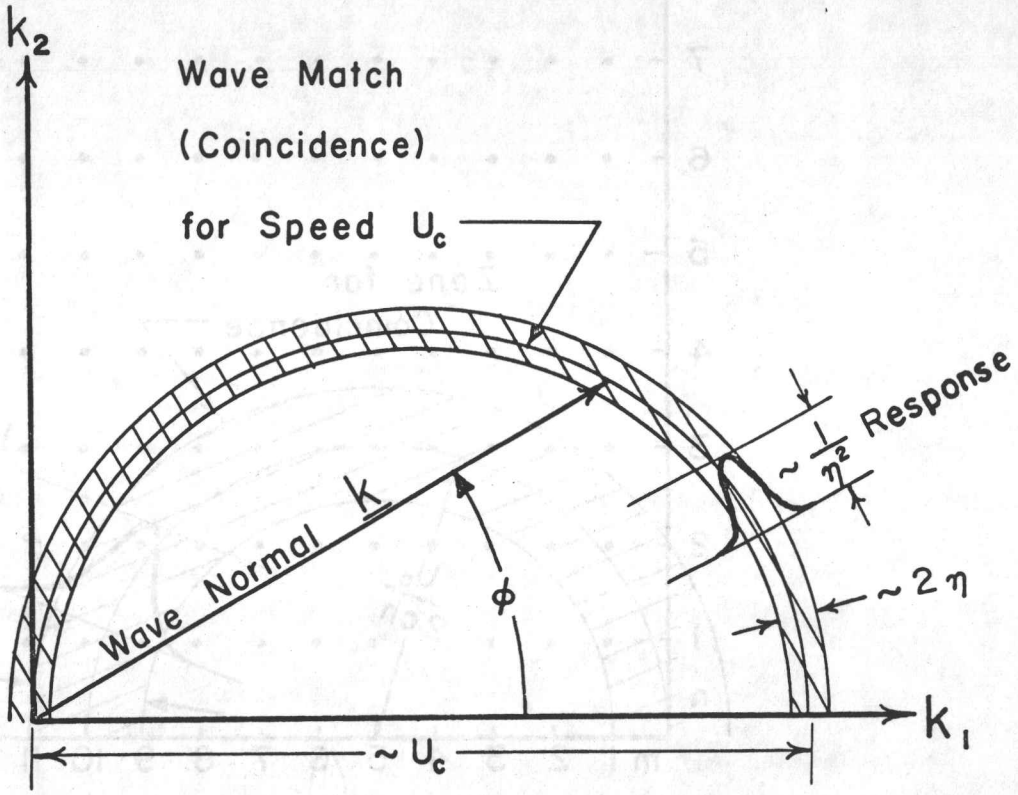

FIGURE 25. LOCUS OF WAVE NORMALS $\underline{k}$ FOR COINCIDENCE RESONANCE OF INFINITE PANEL.

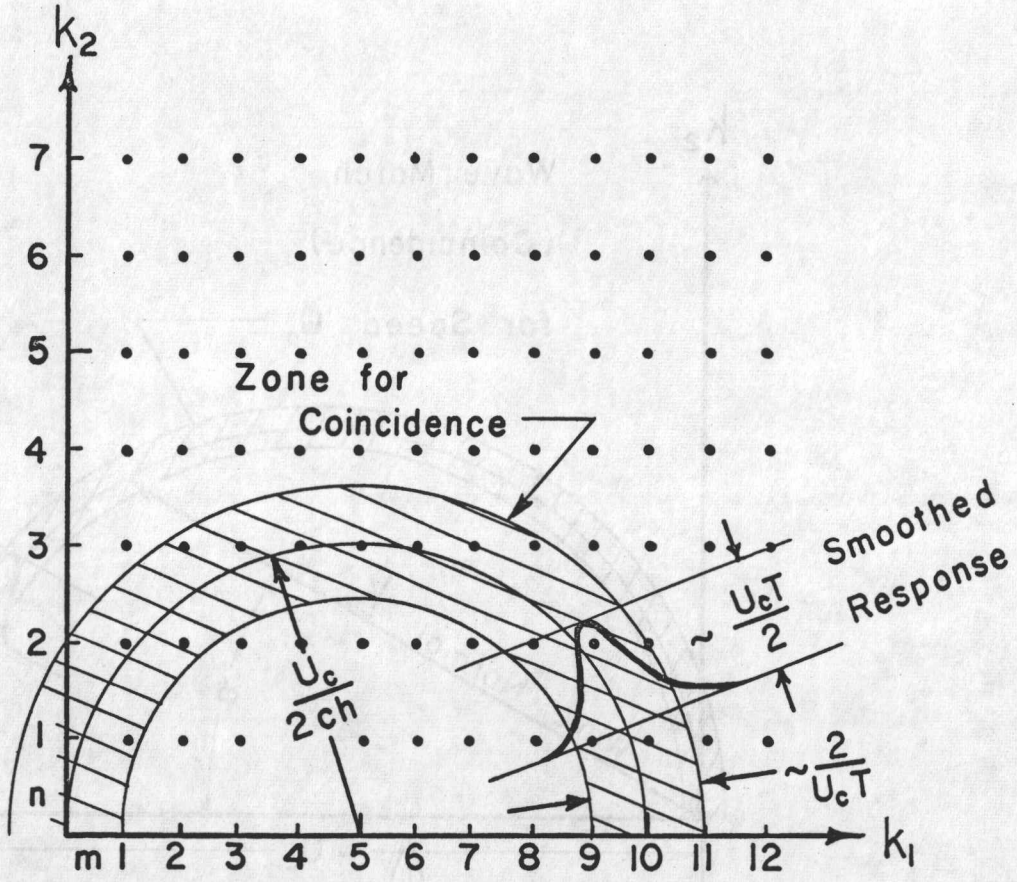

FIGURE 26. MODES m, n OF FINITE PANEL EXCITED BY COINCIDENCE EFFECT {Adapted from [72]}.

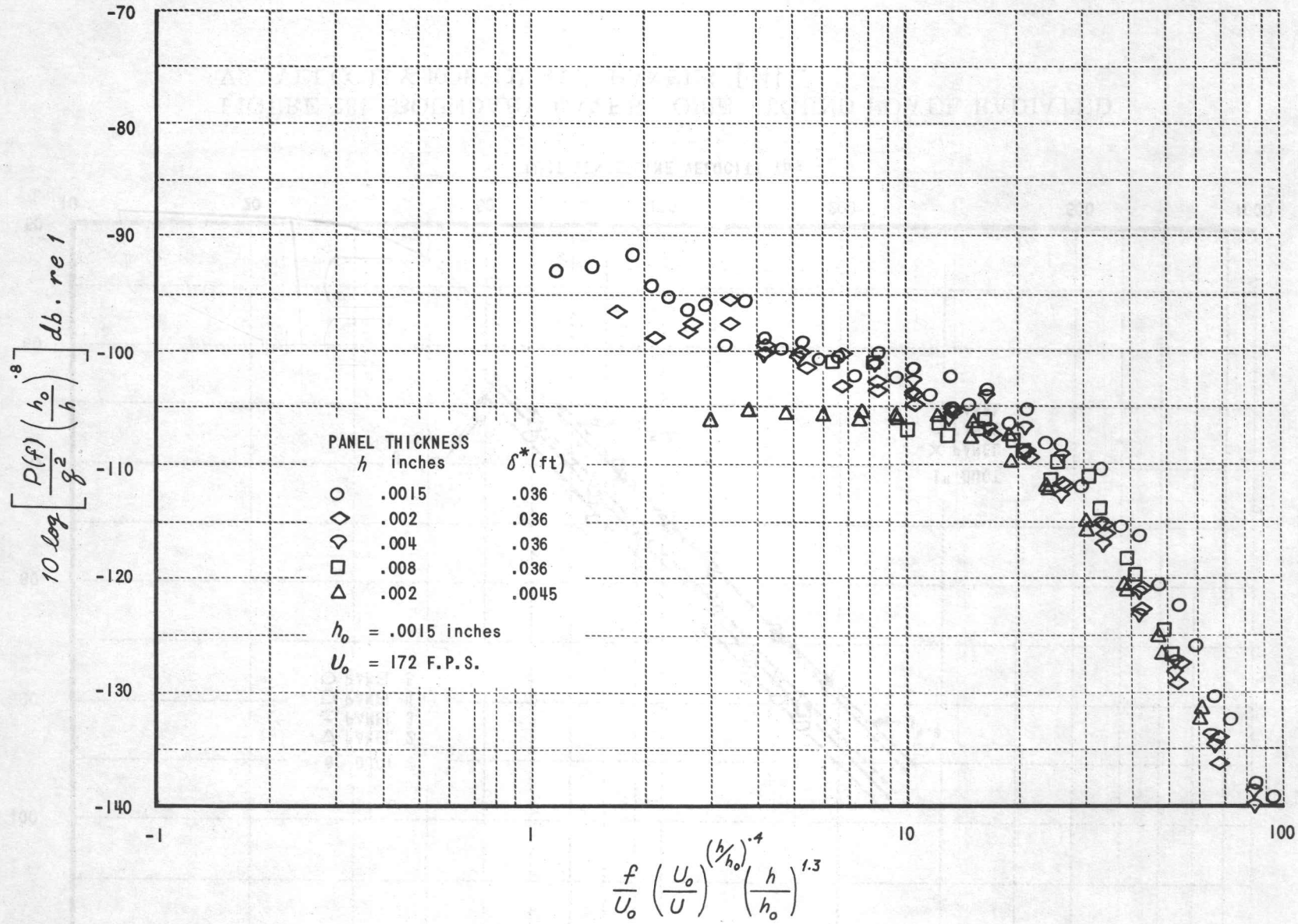

FIGURE 27. UNIVERSAL CURVE OF POWER SPECTRAL DENSITY FOR BOUNDARY LAYER NOISE. 11" x 11" PANELS [94] .

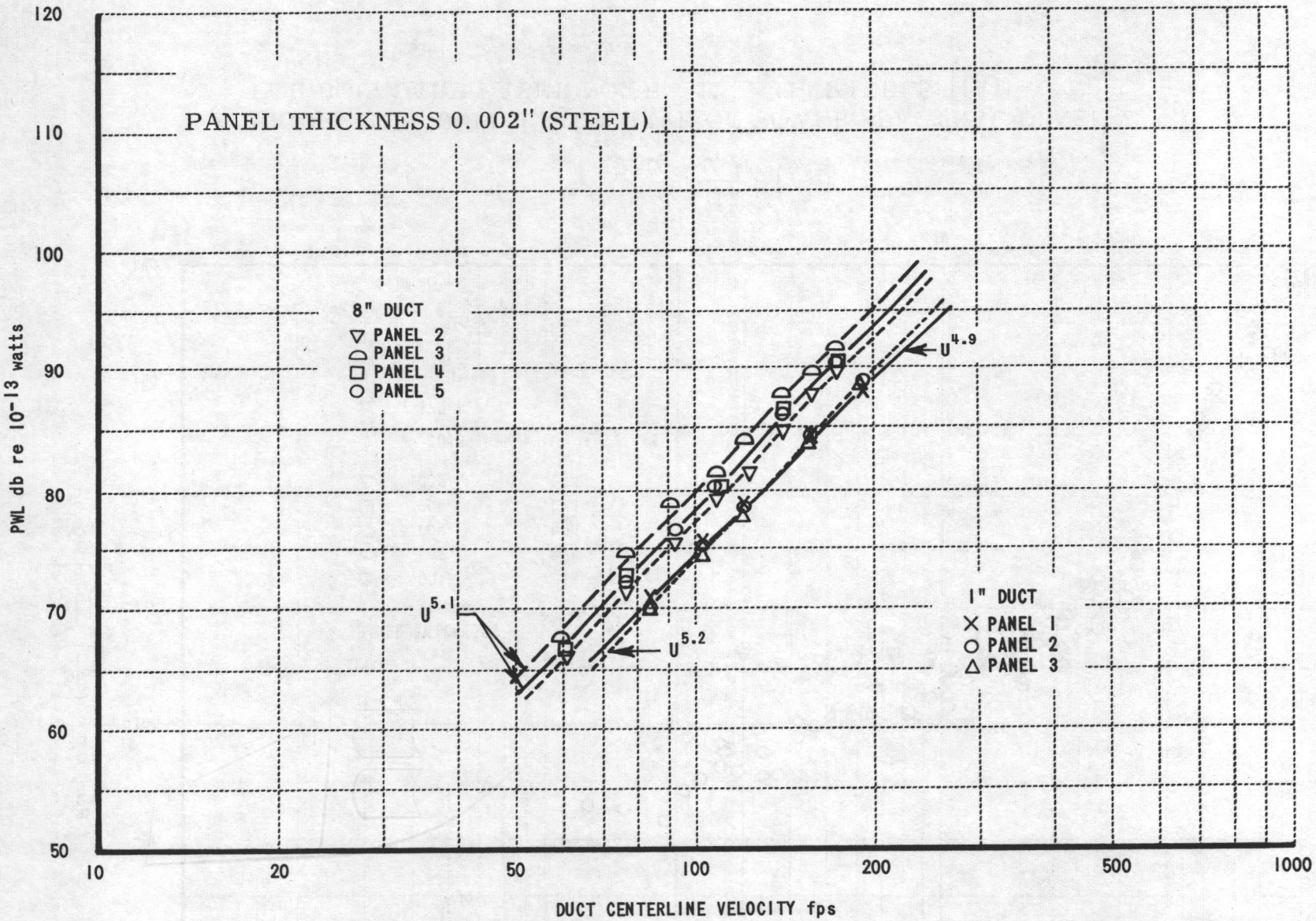

FIGURE 28. BOUNDARY LAYER NOISE. SOUND POWER RADIATED VS. VELOCITY FOR 11" x11" PANELS [94] .

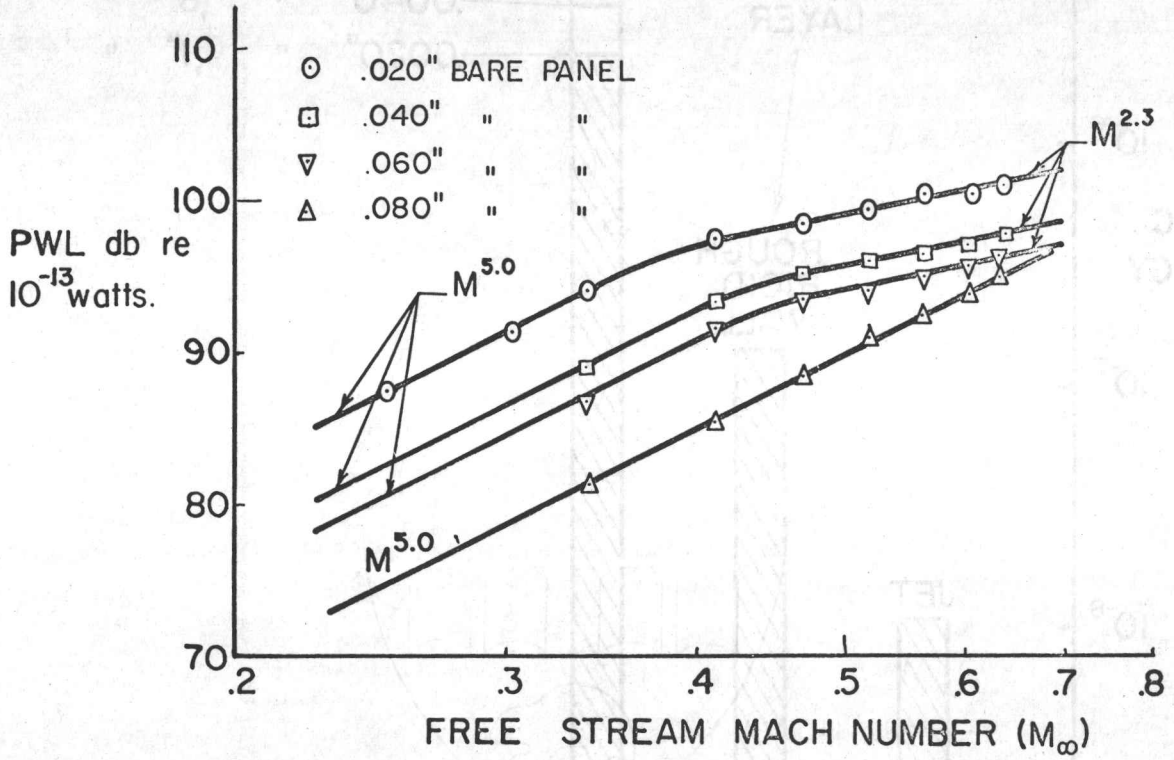

FIG. 29. BOUNDARY LAYER NOISE. SOUND POWER RADIATED VS. VELOCITY FOR 7" X 12" PANELS. [95].

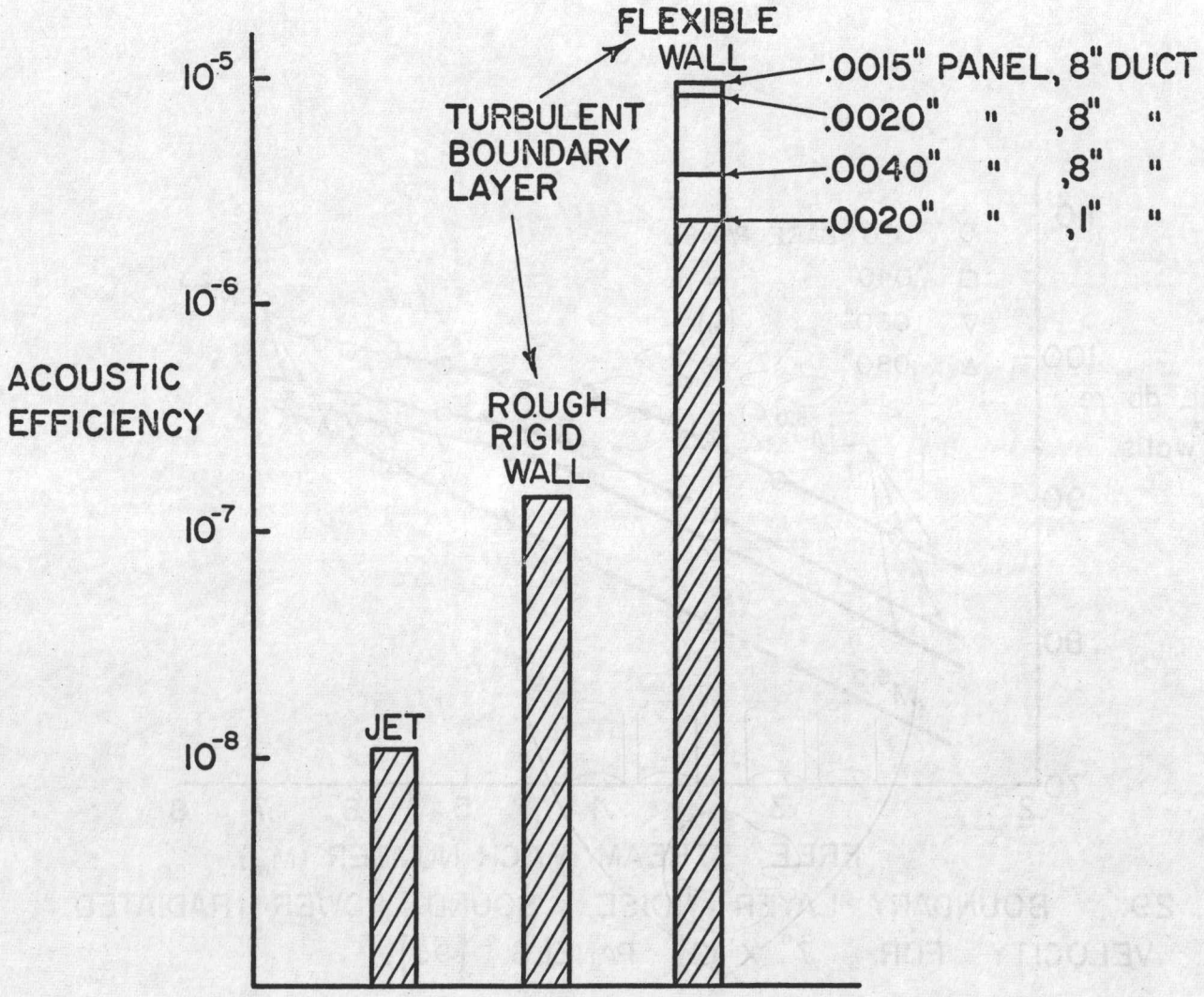

FIG. 30. EFFICIENCIES OF CONVERSION OF MECHANICAL INTO ACOUSTICAL ENERGY AT M = 0.18. (DATA FROM [91] OR [94]).